System Level Design Enhancements for Cost Effective Renewable Power Generation by Reverse Electrodialysis

by

Adam Michael Weiner

B.S.M.E., The Johns Hopkins University (2013)

Submitted to the Department of Mechanical Engineering
in partial fulfillment of the requirements for the degree of

Master of Science in Mechanical Engineering

at the

MASSACHUSETTS INSTITUTE OF TECHNOLOGY

February 2015

Author .....
Department of Mechanical Engineering
January 20, 2015

Certified by .....
John H. Lienhard V
Abdul Latif Jameel Professor
Thesis Supervisor

Accepted by .....
David E. Hardt
Chairman, Committee on Graduate Students

System Level Design Enhancements for Cost Effective Renewable Power Generation by Reverse Electrodialysis

by

Adam Michael Weiner

Submitted to the Department of Mechanical Engineering
on January 20, 2015, in partial fulfillment of the
requirements for the degree of
Master of Science in Mechanical Engineering

Abstract

Studies of the future competitiveness of reverse electrodialysis (RED) with other energy technologies show that the projected levelized cost of electricity realized through current stack designs is prohibitively high. Despite these high projected costs, RED maintains other advantages - namely, the harnessing of a renewable and non-intermittent energy resource, the emissions-free operation, the direct conversion of chemical potential energy to electrical energy, and other environmental merits. Motivated by these advantages, system-level design enhancements and strategies are proposed and analyzed with the primary objective of reducing the projected levelized cost of electricity produced by an RED stack. The combined recommendations presented in this work result in projected cost reductions of over 40%.

A major source of the cost reductions arises through the implementation of a new reverse electrodialysis stack design strategy which prioritizes the minimization of the levelized cost of electricity as opposed to the maximization of stack power density. The shift in strategy not only results in the definition of an optimal stack length which accounts for the trade-off between stack costs and pretreatment costs, but also the identification of an optimal load resistance which accounts for streamwise salinity variations and an optimal feed velocity which accounts for the trade-off between concentration polarization losses and pumping power losses. For all three design parameters, the identified optimum is smaller than what is currently prescribed in the literature.

Further costs reductions are realized by blending the incoming river water feed with a higher salinity stream to reduce the largest source of irreversible losses in the stack - the electrical resistance of the diluate channel. The increase in diluate salinity, however, sacrifices some of the chemical potential between the inlet feeds. This trade-off is analyzed and the optimal inlet diluate salinity is identified for three different stack configurations. In all cases, the optimal salinity is higher than most local river water salinities at promising RED sites, rendering blending beneficial. Furthermore, the development of back-end blending, in which

the diluate exiting the stack is used as the high salinity stream for blending, results in additional pretreatment cost reductions, as the already-pretreated diluate is recycled.

Thesis Supervisor: John H. Lienhard V
Title: Abdul Latif Jameel Professor

Acknowledgments

I would like to thank Professor John Lienhard for dedicating his time to guiding me, challenging me, and supporting me throughout my experience at MIT, and for inspiring in me a lasting interest in global water issues.

One of the main lessons I've learned at MIT is that great mentors can have an enduring influence. Ronan McGovern, thank you for always setting the bar high and for pushing me to succeed. Most importantly, thank you for being a great friend.

I would like to also thank Leo Banchik for his consistent encouragement and unwavering support throughout this experience. You have had a strong impact on me, and you will always be a close friend. I have learned so much from all of my friends and colleagues in the Lienhard Research Group, who bring a passion and energy everyday to the work they do. To each of you, thanks for your motivation and support throughout my time at MIT.

I express my gratitude as well to the King Fahd University of Petroleum and Minerals and the Center for Clean Water and Clean Energy at MIT and KFUPM for financially supporting this work. I have thoroughly enjoyed being a part of this unique collaboration.

I have been truly blessed with a strong and caring family. Mom and Dad, Aaron and Alex, thank you for your unshakable love and encouragement and for instilling in me the values which guide me wherever I go. I love you very much.

THIS PAGE INTENTIONALLY LEFT BLANK

Contents

THIS PAGE INTENTIONALLY LEFT BLANK

List of Figures

THIS PAGE INTENTIONALLY LEFT BLANK

List of Tables

Nomenclature

Roman Symbols

A	area, m^2
C	concentration, mol/m^3
CAF	capital ammortization factor, yrs
D	diffusivity, m^2/s
F	Faraday's constant, C/mol
g	acceleration due to gravity, m/s^2
H	head loss, m
h	channel height, m
J	molar flux, mol/m^2 s
j	current density, A/m^2
K	constant
L	membrane permeability
l	length, m
$LCOE$	levelized cost of electricity, \$/kWh
M	molar mass, kg/mol
NPV	net present value, \$
P	power density, W/m^2
p	pressure, Pa
R	universal gas constant, J/mol K
R	resistance, Ω
r	annuity depreciation rate
$\bar{r}$	membrane surface resistance, Ω m^2
Re	Reynolds number
RED	Reverse electrodialysis
S	salinity, ppm

Sc	Schmidt number
SGP	Salinity gradient power
Sh	Sherwood number
T	temperature, K
t	transport number
V	feed velocity, m/s
w	stack width, m
X	mass-based blending fraction

Greek Symbols

Δ	change
ϵ	local EMF, V
ε	spacer porosity
Γ	number of periods
γ	activity coefficient
κ	conductivity, S/m
Λ	molar conductivity, S m^2/mol
μ	chemical potential, J/mol
μ	viscosity, Pa-s
ρ	density, kg/m^3
ϕ	voltage, V
π	osmotic pressure, bar
Θ	dimensionless stack resistance

Subscripts

AEM	anion exchange membrane
aq	aqueous
avg	average

blend	blended
c	concentrate or critical
cu	counter-ion
CEM	cation exchange membrane
CP	concentration polarization
D	density
D_h	hydraulic diameter
d	diluate
eq	equivalent
g	gross
i	inlet
L	load
m	membrane surface
mem	membrane
N	exit
n	segment number
$NaCl$	salt solution
net	net
OC	open-circuit
opt	optimal
PT	pretreatment
p	pressure
r	river water
s	stack
stack	stack
sw	seawater
tot	total

Superscripts

s	salt
w	water
$*$	without concentration polarization

THIS PAGE INTENTIONALLY LEFT BLANK

Chapter 1

Introduction

Reverse electrodialysis (RED) is an energy production technology which directly converts the chemical potential energy available through a concentration difference to electrical energy used for work. When implemented at the site of a naturally-occurring salinity gradient (an estuary, for example), reverse electrodialysis may be used to produce emission-free, non-intermittent renewable energy. Employed in this fashion, reverse electrodialysis may be classified as a salinity gradient power (SGP) technology.

1.1 Advantages of salinity gradient power

Researchers identify several key advantages of SGP technologies over other energy technologies. Salinity gradient energy is first and foremost a renewable resource. Work is continuously extracted from the Sun-driven hydrological cycle, which may be approximated as a modified Rankine cycle [3]. The available energy is the difference between the heat provided by the Sun to evaporate seawater and the heat expelled in condensing pure water vapor. During operation, SGP processes are also mostly emissions-free (CO_2 or otherwise) and produce saline waste streams which are non-polluting. Thermal pollution is also avoided as the process proceeds at a relatively constant temperature [4].

Another commonly cited motivation for pursuing salinity gradient power is the large

amount of power which could potentially be extracted from river mouths worldwide. While global estimates based on river discharges and salinities place this potential between 1.5 TW [5] and 2.6 TW [6], the utility of such a figure is overstated for two reasons. First, in the spirit of comparing SGP to other renewable energy sources, this global potential is actually quite small. Secondly, although RED systems may be operated at over 80% efficiency [7], the efficiency of an economical process is much lower, because there is a trade-off between efficiency (which determines operating cost) and power density (which determines capital cost). An examination of this trade-off between efficiency and power density with respect to RED design is presented in Chapter 2. At a high efficiency the power density is extremely low and the capital costs of the system are overwhelmingly large. The lowest cost design shown in Chapter 2 operates at an efficiency of 20%. Using this efficiency, the economical potential reduces to, at most, 520 GW globally. When river mouths are carefully evaluated for SGP suitability, this global potential is reduced even further but still remains sizable.

Other advantages of salinity gradient power include its non-intermittent character, enabling the operation of SGP plants at capacity factors close to unity. Issues with intermittency drive the capacity factors of solar, wind, tidal, and wave technologies down, necessitate the employment of storage systems, complicate grid operations, and preclude such technologies from serving as base loads. While changing seawater intrusion lengths, drought, and other weather phenomena introduce some level of unpredictability to salinity gradient power production at river mouths, the expected capacity factors remain much higher. Consistent, predictable electricity production is undoubtedly a strong advantage for salinity gradient power technologies.

Partly because salinity gradient power is non-intermittent, it is often compared favorably to hydroelectric power - another commonly cited motivation for current research. For instance, the chemical potential energy existing between 1 m^3 of river water and 1 m^3 of seawater is equivalent to the gravitational potential energy of 1 m^3 of river water raised 142 m higher than another m^3 of river water [5]. With a hydroelectric conversion efficiency of 90% [8] and an RED efficiency of 20%, the volumetric energy density of an SGP system at a

river mouth is equivalent to the volumetric energy density of a 32 m high dam. For context, over 85% of hydroelectric dams in the United States are less than 32 m tall [9]. Nevertheless, the utility of this figure is limited as well, because the cost of electricity produced by an RED system is driven primarily by the energy produced per m^2 of membrane area not the volumetric energy density of the feed water. This consideration is explored further in Chapter 2.

Salinity gradient power may have distinct advantages over hydroelectric power with respect to environmental and social impacts that have not been considered in the SGP literature. Because SGP plants would be installed at river mouths, operations would not impact downstream communities in the way hydroelectric dams do. In Vietnam, for instance, a national boom in hydropower construction has put villagers at risk of flash floods, destroyed surrounding forests, and deprived farmers of irrigation water in the dry season [10]. Salinity gradient power plants would compete for freshwater as hydroelectric power plants do, but because SGP plants would be installed downstream, they would not have the same ability to deprive farmers of water for irrigation. Additionally, SGP plants could neither cause flash foods nor impact the surrounding ecosystem to the same degree as hydroelectric dams.

1.2 Advantages of reverse electrodialysis

Two salinity gradient power technologies, reverse electrodialysis and pressure-retarded osmosis, show the most promise for eventual commercialization. Capacitive mixing, another SGP technology, is in a more nascent stage of development. Among these technologies, reverse electrodialysis has several distinct advantages which may be understood in the context of the RED system and its operation.

An RED system operates similarly to a concentration cell in that the chemical potential energy existing between two identical substances due to a concentration difference is converted directly to electrical work at a relatively constant temperature. The typical system consists of intake and outlet conduits, a pretreatment system, RED stack, and converter. The RED stack (with cross-section depicted in Fig. 1-1) consists of a pile of alternating

sheets of anion and cation exchange membranes (AEM and CEM) with mesh spacers in between each membrane and two electrodes sandwiching the pile at either end. The spacers form channels between the membranes through which alternating high-salinity concentrate and low-salinity diluate feeds are conveyed. In the channels adjacent to the electrodes, rinse solutions are circulated.

The cation and anion exchange membranes consist of a polymer matrix with fixed acidic or basic dissociating groups inserted to create a fixed-charge distribution. Cation exchange membranes consist of negative fixed charges which electrostatically repel anions and anion exchange membranes consist of positive fixed charges [11]. For the electrodes, Veerman et al. [4] recommend graphite electrodes to reduce cost and reduce gas formation in the rinse (which leads to voltage losses) in combination with a rinse solution consisting of a Fe^{2+}/Fe^{3+} redox couple in an NaCl-HCl supporting electrolyte. Fe^{2+} and Fe^{3+} concentrations are maintained through mixing and recirculating the rinse solutions.

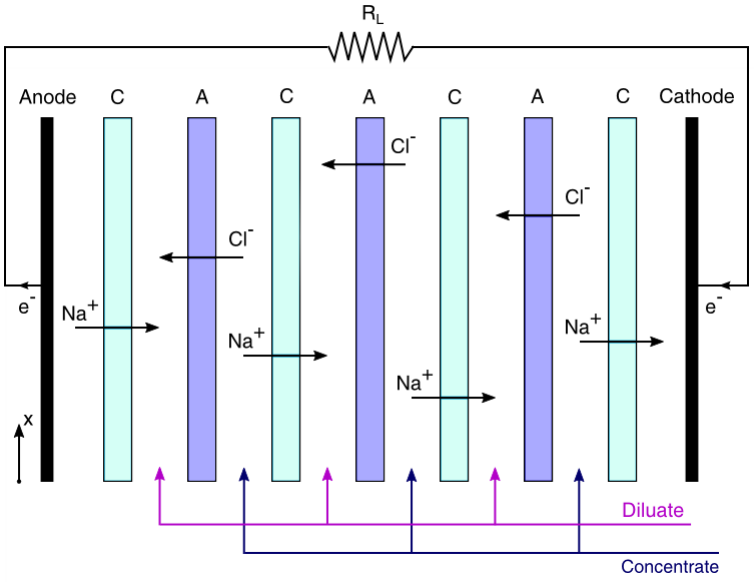

Figure 1-1: A schematic diagram of a typical reverse electrodialysis stack

The concentration gradient persisting between the channels drives cations from the concentrate through the CEM membranes towards the cathode and anions from the concentrate through the AEM membranes towards the anode. The charge separation creates membrane

potentials which add together in series across the stack. The net ionic current which persists is converted to electric current at the electrodes via a redox reaction pair.

The RED energy conversion process has several advantages over PRO. First, the direct conversion of chemical potential to electrical work eliminates the extra losses associated with converting chemical potential to mechanical work and then mechanical work to electrical work. Post et al. [12] have shown through modeling current and projected designs that RED delivers a higher power density and efficiency than PRO for river and sea water feeds. RED also benefits from fewer moving parts which reduces the complexity of operation and likely results in less maintenance. Furthermore, the impact of fouling on RED performance may be less than in PRO, because the membranes are generally more resistant and easier to clean [12]. Vermaas et al. [13] have shown that feedwater reversal, where the polarity of the RED stack is periodically flipped, in combination with air-sparging are promising methods for preventing colloids and organic acids from fouling the membranes.

1.3 Challenges in competing with other renewables

Many of the challenges facing reverse electrodialysis in competing with other renewable energy technologies are shared by the other salinity gradient power technologies. Among them is a lack of truly suitable river mouth locations worldwide. Suitability is a function of salinity structure primarily, a characteristic studied recently by Alvarez-Silva et al. [14]. River mouths with strongly stratified and salt-wedge salinity structures, brought about by weak tidal forcing and a large discharge, are the most promising sites. Of the 20 major global river systems featured in the study, eight are deemed suitable and seven at least partially suitable based on these criteria. Another characteristic of river mouth suitability is the feed water fouling potential. Many river mouth environments in the low latitudes, for instance, support increased biological activity and sedimentation, posing costly fouling risks [5]. Temperature is another important characteristic. Low temperature climates reduce the Gibbs free energy difference and conductivity of the feed water streams [15].

Other environmental concerns pose challenges to the implementation of SGP technolo-

gies. As with traditional desalination plants, the disruptive impact of fresh and sea water withdrawal and discharge on marine life is a concern as well as, in many places, the cost and complications associated with coastal permitting. Additionally, global warming trends are pushing salt intrusion lengths deeper into freshwater rivers as well as increasing the frequency and severity of droughts. Together, these effects are reducing the suitability of many potential SGP sites.

But perhaps the most significant and immediate challenge is to reduce the cost of electricity produced by SGP systems. The projected cost of electricity produced by a typical RED system remains prohibitively higher than the average electricity cost from other renewable energy technologies [16]. As we discuss in Chapter 2, the primary cost drivers in reverse electrodialysis are: the low gross power density of an RED stack, the costly energy requirement of pretreatment and/or antifouling methods as well as pumping systems, and the current price of ion exchange membranes. Over time, the price and production cost of ion exchange membranes will fall with increasing scale and improved manufacturing techniques [5]. However, the other cost drivers will only be addressed with persistent research and new innovations in various areas. System-level design enhancements represent one area which has the strong potential to deliver significant improvements.

1.4 Motivation for this thesis

The initial motivation for the RED system design study as discussed in Chapter 2, is an absence in the literature of a reasonable strategy for determining the optimal length of an RED stack. Across the literature, RED design parameters have been chosen based on optimizing performance as opposed to cost, with objectives ranging from maximizing the gross power density of the stack to maximizing the river water yield. In all of these cases the conventional wisdom is to make the stack length as small as possible to increase the power density; a stack length of 10 cm is typical. Such approaches do not account for maximizing the stack efficiency to minimize the cost of pretreatment - a strategy which favors large stack lengths.

By shifting the design objective to minimizing the levelized cost of electricity, the trade-off between power density and efficiency is captured, and all performance objectives are consolidated into a single objective function. Through developing a cost model and optimization procedure, we identified the optimal stack length as well as the optimal load resistance and feed velocity for a typical RED stack design. Under current price conditions, each optimal design parameter is smaller than what is currently presented in the literature. Additionally, we provide a simple RED cost model which accounts for pretreatment, a justification for optimizing load resistance, and an explanation of the primary trade-offs determining each optimal design parameter.

In the process of determining the optimal design parameters, we identified an opportunity for increasing the gross power density of an RED stack by blending the diluate feed with a higher salinity stream before the stack entrance. This design enhancement, which we simply term *blending*, is explained and analyzed in Chapter 3. That chapter also examines the expected reductions in the levelized cost of electricity for two different system configurations.

The concept of blending arose after examining the trade-off between stack voltage and stack current with respect to the diluate feed salinity. As the inlet diluate feed salinity rises relative to the inlet concentrate salinity, the salinity gradient and chemical potential difference falls, driving the stack voltage lower. Concurrently however, the resistance of the diluate channel falls, driving the stack current higher. We find that the optimal diluate salinity for a range of stack designs is significantly higher than the salinity of most rivers deemed suitable for RED and that the potential power density improvements and cost reductions through blending are sizable. We also show that additional cost reductions may be realized by using the diluate exit feed as the high salinity stream to blend with the river water feed. This reduces pretreatment costs, because much of the already-pretreated diluate feed is recycled in the blending process.

THIS PAGE INTENTIONALLY LEFT BLANK

Chapter 2

A new reverse electrodialysis design strategy which significantly reduces the levelized cost of electricity

Summary

In this chapter [1], we develop a framework for choosing the optimal load resistance, feed velocity, and stack length for a reverse electrodialysis stack based on minimizing the levelized cost of electricity. The optimal load resistance maximizes the gross stack power density and results from a trade-off between a large stack voltage and a large stack current. The primary trade-off governing the optimal feed velocity is between stack pumping power losses which reduce the net power density and concentration polarization losses which reduce the gross stack power density. Lastly, the primary trade-off governing the optimal stack length is between the capital costs of the stack and pretreatment system. Implementing our strategy, we show that a smaller load resistance, stack length, and feed velocity than what is currently proposed in the literature reduces costs by over 40%. Despite these reductions, reverse electrodialysis remains more costly than other renewable technologies.

[1] The author acknowledges contributions from Ronan McGovern to the work in this chapter

2.1 Introduction

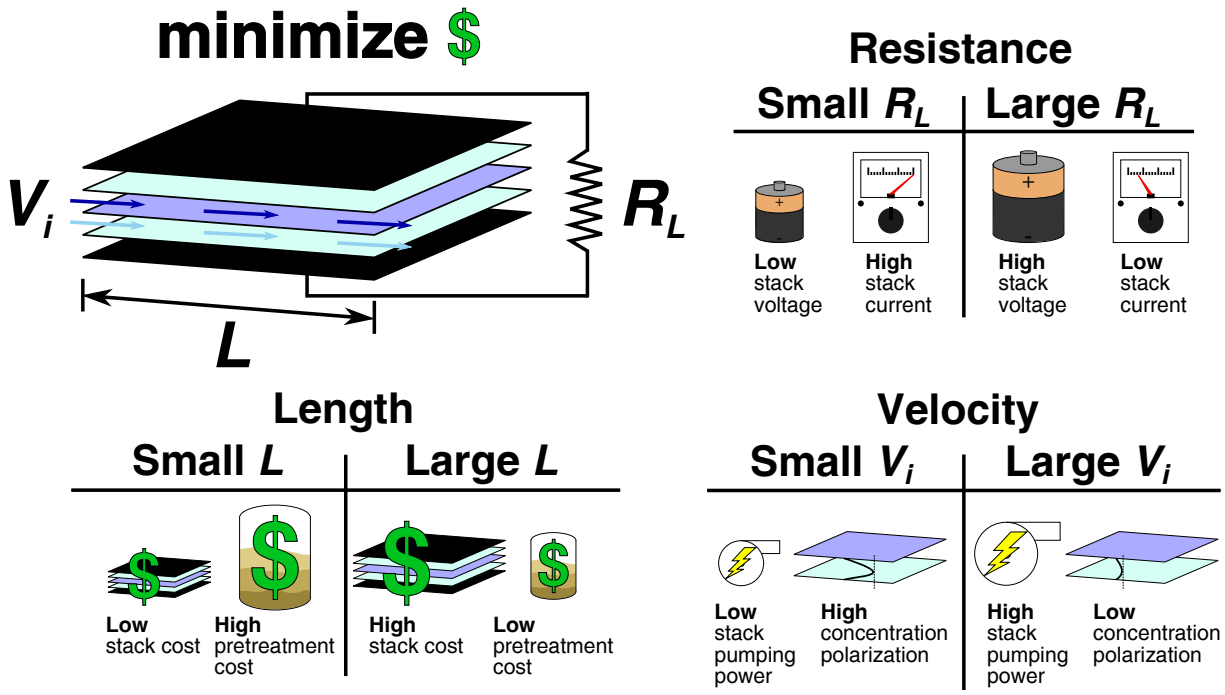

Figure 2-1: The primary trade-offs associated with determining the optimal load resistance R_L, optimal stack length L, and optimal inlet feed velocity V_i which minimize the levelized cost of electricity.

A reverse electrodialysis stack consists of alternating layers of anion and cation exchange membranes sandwiched between two electrodes, which are connected in series to an external load resistor. Diluate and concentrate feeds are pumped between the layers, facilitating ion transfer along the membrane length and converting the chemical potential stored in the salinity gradient to electrical work. In the literature, aspects of the overall system performance [17], stack design [18], and membrane characteristics [19] have been explored extensively. Studies to date have allowed for improvements in stack power density, net power density, and efficiency through the consideration of smaller channel heights [1], profiled membranes [20], and ion conductive spacers [21]. By contrast, the objective of this chapter is to determine the optimal load resistance, stack length, and feed velocity - important design parameters for a typical seawater/freshwater configuration - based on minimizing the

levelized cost of electricity produced.

In the literature, the optimal load resistance is chosen by setting it equal to the equivalent stack resistance, as in traditional impedance or load matching, to maximize the power density delivered by the stack (the gross power density) [1, 7, 20]. We show that in fact traditional load matching does not maximize the gross power density, because the stack resistance is itself a function of the load resistance. Instead, we propose a more rigorous numerical maximization of the gross power density to determine the optimal load resistance. Additionally, we show that the load resistance which maximizes the gross power density also minimizes the levelized cost of electricity.

Unlike for the load resistance, a method for determining the optimal stack length currently does not exist in the literature. Most RED designs employ very small stack lengths (typically 10 cm [1, 22]), because this approximately maximizes the gross power density. As the length increases, more salt is transported from the concentrate to the diluate, reducing the average salinity difference between the streams. This decreases the average electromotive force along the stack, decreasing the power density. Short stacks maximize power density.

Long stacks, however, maximize efficiency. As more salt is transported, more of the initial chemical potential energy between the streams is converted to electrical energy. From an economic perspective, this reduces pretreatment costs. Long stacks minimize pretreatment costs. Other RED designs consider the trade-off between efficiency and power density, yet none argue for a specific optimal length. Recently, for example, Yip et al. [17] quantify how efficiency and power density each vary with length. Veerman et al. [18] take a step further by arguing for a specific objective function - the response product - which squares the net power density and divides by the river water flow rate.

We argue for a specific optimal stack length based on the minimization of the levelized cost of electricity. The advantage is that the trade-off between power density and efficiency is captured in a well-motivated objective function. The capital cost per unit of net power output increases with decreasing stack length due to increasing power density. However, with decreasing stack length, pretreatment costs per unit of net power output rise due to

decreasing efficiency.

A method for determining the optimal feed velocity of the concentrate and diluate streams is identified in the literature, chosen based on a trade-off between the gross power density and the power consumed in pumping the feeds through the stack [1, 22]. As the feed velocity decreases, more salt is transported from the concentrate to the diluate. As with longer stack lengths, this reduces the average salinity difference between the streams, decreasing the gross power density. In addition, concentration polarization losses increase non-linearly with decreasing velocity. Hence, large velocities maximize gross power density.

Small velocities, however, minimize the power consumed in pumping the feeds through the stack. A few previous studies in the literature have identified an optimal operating flow velocity based on this trade-off between gross power density and pumping power density. Vermaas et al. [1], for example, experimentally identify an optimal feed velocity of 1 cm/s for a typical stack design with 100 μm channel heights.

We argue that the optimal velocity must also account for efficiency. With respect to velocity, when power density increases, efficiency increases. Hence, large velocities maximize efficiency, reducing pretreatment costs. To our knowledge, no calculation of the optimal stack velocity in the literature has accounted for efficiency. As with the optimal stack length and load resistance, we argue for an optimal stack velocity based on the minimization of the levelized cost of electricity. In this way, we account for the effect of velocity on gross power density, pumping power, as well as efficiency. We also account for the energy consumed in pumping the feeds through the pretreatment system.

In sum, our design strategy suggests choosing a load resistance and feed velocity which are significantly smaller than what is found in the literature and a stack length which is slightly smaller. Figure 2-1 summarizes the key insights of this chapter - namely, the primary trade-offs associated with determining the optimal load resistance, stack length, and feed velocity according to our strategy.

2.2 Methodology

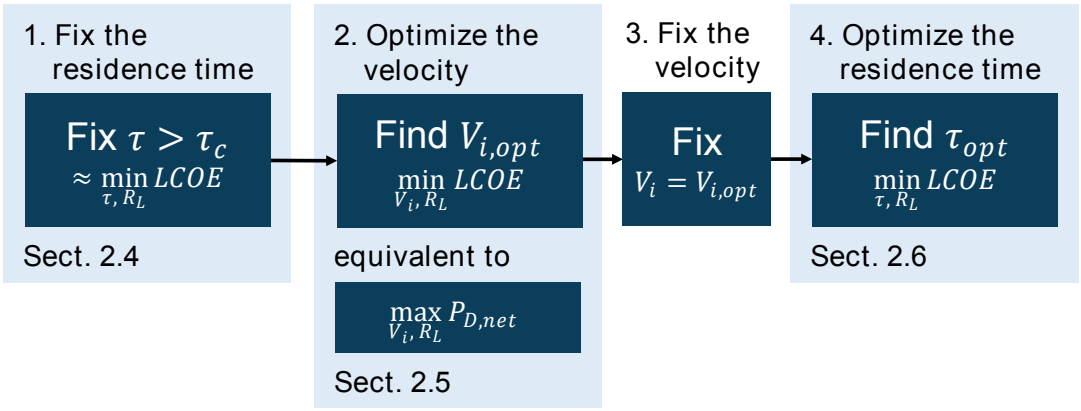

Figure 2-2: An optimization method for RED stack design, where τ is the residence time and τ_c is the critical residence time, $LCOE$ is the levelized cost of electricity, R_L is the load resistance, and V_i is the inlet feed velocity.

Figure 2-2 illustrates our recommended optimization approach for designing an RED stack. First we fix the residence time τ (the stack length divided by the feed velocity) at an arbitrary value significantly larger than a critical residence time τ_c. While holding the residence time fixed, we minimize the levelized cost of electricity with respect to feed velocity and load resistance. Because the residence time is fixed, the stack length is implicitly varied as well. We show that this optimization step is equivalent to maximizing the gross power density with respect to the load resistance and maximizing the net power density with respect to the feed velocity. Then we fix the feed velocity and minimize the cost with respect to residence time and load resistance. Again, the stack length is implicitly varied in this step. Together, the optimal feed velocity and residence time yield the optimal stack length.

In our analysis, we hold the diluate and concentrate channel heights constant and equal at 100 μm - the optimal channel height with respect to net power density identified by Vermaas et al. [1]. While smaller channel heights increase the gross power density, they also increase pumping power losses as well as manufacturing difficulty. Larger channel heights significantly reduce the gross power density. The sensitivity of our results to channel height

is explored in Sect. 2.6.1. We set the feed velocities equal and channel heights equal to simplify the system design. We suggest that the greatest cost reductions can be achieved through optimizing the load resistance, stack length, and feed velocity.

The first step in calculating the levelized cost of electricity for the optimization procedure is to model the net power density of the system - the gross power density less the pumping power density consumed in the pretreatment (PT) system and the stack. Our method is illustrated in Fig. 2-3. In Sect. 2.3, we show that the load resistance which maximizes the gross power density also minimizes the levelized cost of electricity. Hence, in modeling the gross power density we always maximize with respect to the load resistance.

The gross power density model itself is of an unsegmented-electrode RED stack, validated with experimental results from the literature. The model is one-dimensional, accounting for streamwise variations in salinities, membrane potentials, and channel resistances along the stack. We base the model for pumping power consumed in the pretreatment system and stack on systems reported in the literature. All equations were solved numerically using a quadratic approximation method in Engineering Equation Solver [23].

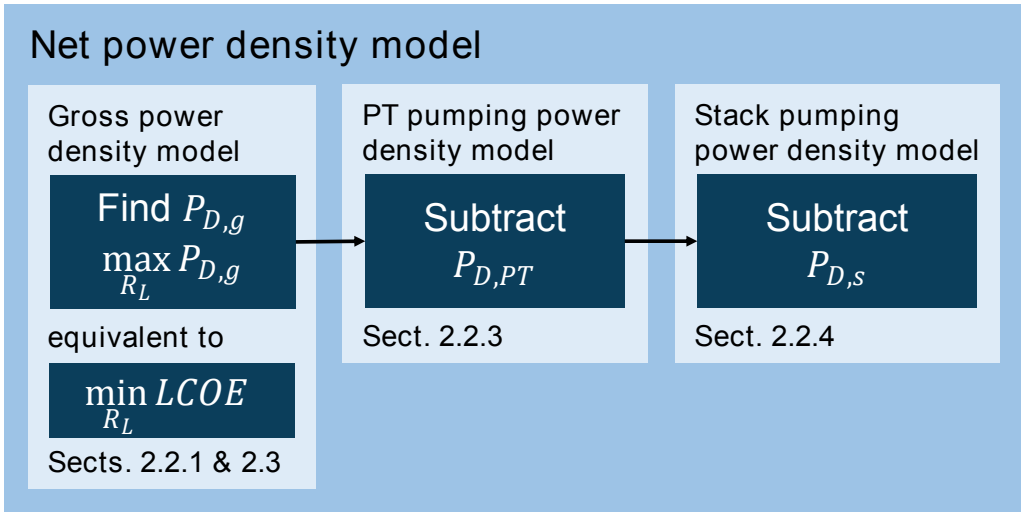

Figure 2-3: The net power density of the system $P_{D,\text{net}}$ is the gross power density $P_{D,g}$ supplied by the stack, continuously maximized with respect to the load resistance R_L, less the power densities consumed in pumping the feed through the pretreatment system $P_{D,PT}$ and stack $P_{D,s}$.

2.2.1 Model for gross power density

Figure 2-4 shows how the circuit was modeled to determine the gross power density. An RED cell pair is divided along the length L into N discrete segments to capture streamwise variations in concentration. Each segment is connected in parallel via the unsegmented electrodes on either side. The electrodes are joined in series with a single, external load resistor. We model neither ionic shortcut currents nor voltage losses to chemical reactions at the electrodes. In stacks with many cell pairs in series, the voltage loss at the electrodes is negligible relative to the sum of the membrane potentials.

Because the concentration of the diluate and concentrate streams vary along the stack length, each segment has an associated local electromotive force (EMF) ε_n effectively connected in series with membrane surface resistances ($\bar{r}_{\mathrm{AEM}}$ and $\bar{r}_{\mathrm{CEM}}$) and local channel resistances ($\bar{r}_{d,n}$ and $\bar{r}_{c,n}$). We assume the membrane surface resistances are constant along the length.

The local EMFs ε_n are computed from the local chemical potential differences across the membranes:

$$\varepsilon_n = \frac{t_s}{F}\left(\mu^s_{c,n} - \mu^s_{d,n}\right) + \frac{t_w}{F}\left(\mu^w_{c,n} - \mu^w_{d,n}\right) \tag{2.1}$$

where t_s is the salt transport number, F is Faraday's constant, $\mu^s_{c,n}$ is the local salt chemical potential at the membrane surface on the concentrate side, and $\mu^s_{d,n}$ is the local salt chemical potential at the membrane surface on the diluate side. The difference in concentration between the channel bulk and membrane surface due to concentration polarization was computed using a convection-diffusion model [11] (diluate example shown):

$$C_{d,m,n} - C_{d,n} = \frac{2h_d}{\mathrm{Sh}_{d,n}} \frac{j_{D,n}}{F} \frac{(\bar{T}_{cu} - t_{cu})}{D_{\mathrm{NaCl}}} \tag{2.2}$$

where $C_{d,m,n}$ is the local diluate concentration at the membrane, $C_{d,n}$ is the local diluate concentration in the bulk, $j_{D,n}$ is the local current density (see Eq. 2.5 below), h_d is the diluate channel height, t_{cu} is the counter-ion transport number ($\approx$0.5 for anions and cations),

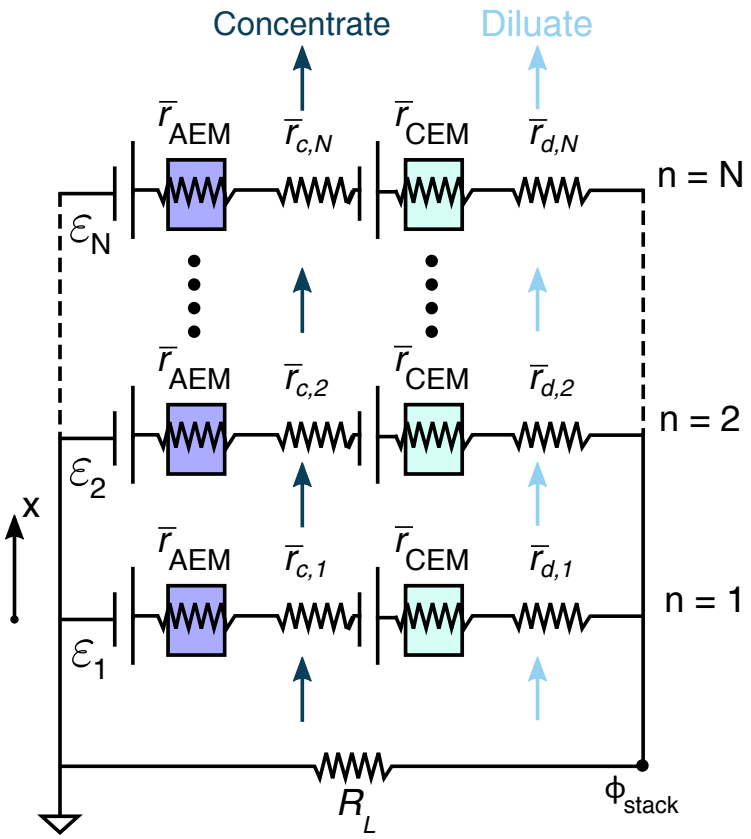

Figure 2-4: A circuit model for the one-dimensional, unsegmented-electrode RED stack which accounts for streamwise variations in concentration.

and D_{NaCl} is the diffusion coefficient of salt through the bulk. $\bar{T}_{cu}$ is the integral counter-ion transport number in the membrane, accounting for migration and diffusion [24]:

$$\bar{T}_{cu} \approx \frac{t_s + 1}{2} \tag{2.3}$$

$\mathrm{Sh}_{d,n}$ is the local Sherwood number, modeled by Kuroda et al. [25] (diluate example shown):

$$\mathrm{Sh}_{d,n} = K_m \mathrm{Re}_{D_h,d,n}^{1/2} \mathrm{Sc}_{d,n}^{1/3} \tag{2.4}$$

where K_m is the Kuroda constant, $\mathrm{Re}_{D_h,d,n}$ is the local Reynolds number based on the hydraulic diameter D_h, and $\mathrm{Sc}_{d,n}$ is the local Schmidt number. The local current density

was modeled as:

$$j_{D,n} = \frac{\varepsilon_n - \phi_{\text{stack}}}{\bar{r}_{tot,n}} \tag{2.5}$$

where ϕ_{stack} is the stack voltage and $\bar{r}_{tot,n}$ is the total local surface resistance, given by [22]:

$$\bar{r}_{tot,n} = \bar{r}_{\text{AEM}} + \bar{r}_{\text{CEM}} + \bar{r}_{d,n} + \bar{r}_{c,n} \tag{2.6}$$

The local channel resistances $\bar{r}_{d,n}$ and $\bar{r}_{c,n}$ are modeled as [22] (diluate example shown):

$$\bar{r}_{d,n} = \frac{h_d}{\epsilon^2 \kappa} \tag{2.7}$$

where ϵ is the spacer porosity and κ is the solution conductivity - the bulk concentration times the solution conductance [26]. An open spacer is described by a spacer porosity ϵ of unity. The opposite is true for a solid spacer [22]. Summing up the local current densities $j_{D,n}$ and applying Kirchoff's Current Law yields an expression for the total stack voltage ϕ_{stack}:

$$\phi_{\text{stack}} = \frac{\sum \frac{\varepsilon_n}{\bar{r}_{tot,n}} A_n}{\frac{1}{R_L} + \sum \frac{1}{\bar{r}_{tot,n}} A_n} \tag{2.8}$$

where A_n is the area of a segment.

The local molar salt and water fluxes $J_{s,n}$ and $J_{w,n}$ transported into the diluate channel are modeled as the sum of migration and diffusion terms based on an approach taken by Fidaleo and Moresi [27]:

$$J_{s,n} = t_s \frac{j_{D,n}}{F} + L_s(C_{c,m,n} - C_{d,m,n}) \tag{2.9}$$

$$J_{w,n} = t_w \frac{j_{D,n}}{F} - L_w(\pi_{c,m,n} - \pi_{d,m,n}) \tag{2.10}$$

where L_s is the overall salt permeability (in m/s), t_w is the water transport number, L_w is the overall water permeability (in mol/bar-m^2-s), and $\pi_{m,n}$ is the local osmotic pressure at the membrane surface [28]. Finally, the gross power density $P_{D,g}$ is given by:

$$P_{D,g} = \frac{\phi_{\text{stack}}^2}{R_L w l} \tag{2.11}$$

where w is the stack width and l is the stack length.

The constants used in the model are compiled in Sect. 2.2.8. To determine the salt and water permeabilities, salt transport number, and Kuroda constant, the model is fit to experimental data [1], see Sect. 2.2.6.

2.2.2 Modeling the open-circuit voltage in an RED stack

The open-circuit voltage ϕ_{OC} in an RED stack with a single electrode is given by setting the load resistance equal to infinity in Eq. 3.12 (or equivalently, setting the total current density in the circuit $j_{D,\text{tot}}$ to zero):

$$\phi_{OC} = \frac{\sum \frac{\varepsilon_n}{\bar{r}_{tot,n}} A_n}{\sum \frac{1}{\bar{r}_{tot,n}} A_n} \tag{2.12}$$

Despite the absence of a *total* current density $j_{D,\text{tot}}$ (the sum of all local current densities through the stack), there is still a positive total salt flux into the diluate channel across the entire length of the stack (see the solid lines in Figs. 2-5 and 2-6). The salt flux arises for two reasons. First, regardless of the presence of local current densities, some salt diffuses into the diluate channel due to membrane imperfections (diffusive flux represented by the dotted lines in Figs. 2-5 and 2-6). Because there is no power extracted from or delivered to the system, the salinity profiles in both the high velocity and low velocity cases are nearly the same. Consequently, the diffusive fluxes are similar.

The flux due to migration arises from local current densities along the stack. Positive current densities form in the front half of the stack and are canceled by negative current densities in the back half. This results in positive local migration in the front half and negative local migration in the back half of the stack (see the dashed lines in Figs. 2-5 and 2-6).

The reason for the rapid rise in open-circuit voltage at low velocities [20] is the rapid

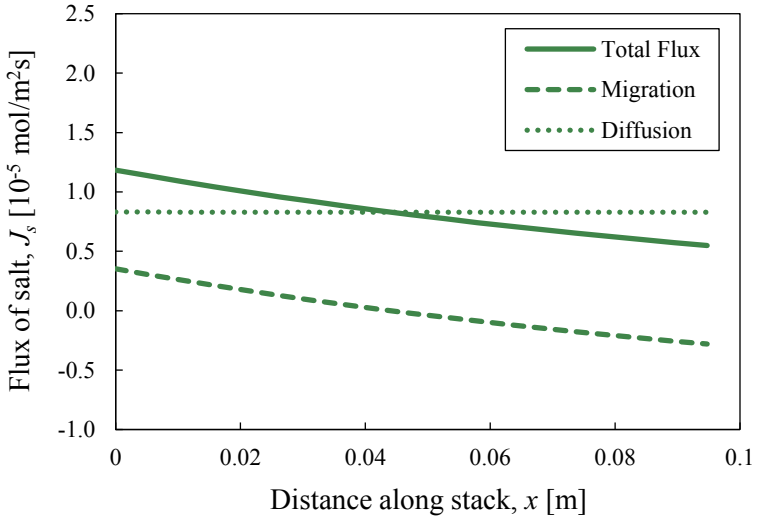

Figure 2-5: Total salt flux in the low velocity (0.25 cm/s) open-circuit case, divided into a migrative flux and a diffusive flux

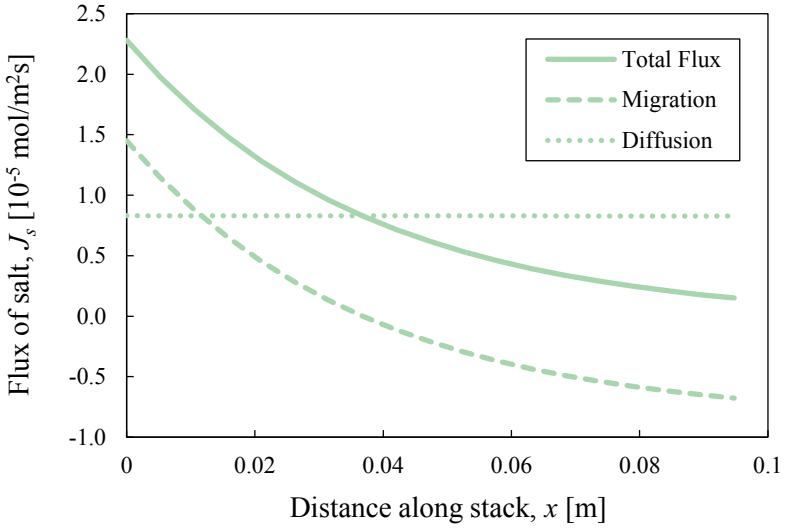

Figure 2-6: Total salt flux in the high velocity (1.25 cm/s) open-circuit case, divided into a migrative flux and a diffusive flux

increase in local EMFs ε_n at higher velocities. With similar average total salt fluxes in the low and high velocity cases, there is less total salt transferred in the high velocity case, resulting in larger salinity gradients along the length and greater local EMFs. The open-circuit voltage plateaus as the total salt transferred becomes effectively zero, approaching

the zero-dimensional stack.

2.2.3 Model for pretreatment system pumping

The pretreatment system is based on a setup suggested by Post et al. [29]. It consists of coarse media-filtration in the form of two rotating drum filters, with light chlorination (1 ppm). We assume a constant, average head loss H of 3.66 m through each drum. The pressure drop is multiplied by the flow rate and divided by the total membrane area to compute a consumed power density for pumping each feed (concentrate and diluate) through the pretreatment system $P_{D,PT}$:

$$P_{D,PT} = \frac{\rho g H h}{\tau} \tag{2.13}$$

where ρ is the feed density, g is the acceleration due to gravity, and τ is the residence time.

2.2.4 Model for stack pumping

The energy cost associated with pumping the concentrate and diluate through the stack is also computed as a power density $P_{D,s}$. The pressure drop across the stack is fit to experimental data [1], see Sect. 2.2.7. Multiplying by the flow rates and dividing by the total membrane area yields the following expression:

$$P_{D,s} = \frac{K_p \mu V_i^2}{h} \tag{2.14}$$

where K_p is a fit parameter and μ is the feed viscosity.

2.2.5 Model for system cost

The cost model was based on the approach taken for electrodialysis by McGovern et al. [30]. The levelized cost of electricity $LCOE$ is defined as the net present value NPV of the system divided by the net power output times the capital amortization factor CAF:

$$LCOE = \frac{\text{NPV}}{(P_{D,\text{net}} wl)\text{CAF}} \tag{2.15}$$

where the net power density $P_{D,\text{net}}$ is given by:

$$P_{D,\text{net}} = P_{D,g} - P_{D,PT} - P_{D,s} \tag{2.16}$$

and the capital amortization factor is given by:

$$\text{CAF} = \frac{1}{r}\left[1 - \left(\frac{1}{1+r}\right)^{\Gamma}\right] \tag{2.17}$$

We assume a plant life of 20 years (Γ in periods) and an annualized cost of capital r of 6% [29]. The net present value consists of a capital contribution for the RED stack and a capital contribution for the pretreatment system. Bundled into the pretreatment capital cost is an operating expense contribution, namely chemical costs associated with pretreatment:

$$\text{NPV} = K_{mem} wl + 2K_{PT} Vhw \tag{2.18}$$

where K_{PT} is the pretreatment system capital cost figure in \$/(m^3/day), and K_{mem} is the RED stack capital cost figure in \$/m^2.

We use a capital cost figure for the pretreatment system K_{PT} of \$20/(m^3/day), which includes operating costs. The capital cost of the pretreatment system is computed by dividing the total construction costs by the operating flux of the system developed by Post et al. [29]. The chemical cost figure is computed assuming light chlorination (1 ppm) is employed on both streams at a cost of \$0.33/kg [31].

We use a capital cost figure for the RED stack K_{mem} of \$750/m^2 [32]. This includes membrane, electrode, frame, and installation costs. In just looking at the membrane material cost, Turek et al. [33] recommend a figure of \$100/m^2 while Daniilidis et al. [16] adopt a membrane price of €50/m^2 for the analysis.

Simplifying the expression for the levelized cost of electricity and rewriting it in terms of

the residence time τ instead of the length yields the following:

$$LCOE = \frac{1}{P_{D,\text{net}}} \left(\frac{K_{mem}}{\text{CAF}} + 2\frac{K_{PT} h}{\tau \text{CAF}} \right) \tag{2.19}$$

Two advantages are gained by framing the net power density and cost models in terms of residence time and velocity as opposed to length and velocity. In Eq. 2.19, fixing the residence time and optimizing for velocity (Steps 1 and 2, Fig. 2-2) simplifies the objective from minimizing cost to maximizing net power density. Additionally, to first order, fixing the residence time fixes total salt transport through the membrane. Hence, the gross power density rises with velocity, solely because concentration polarization losses decrease.

2.2.6 Validation of the gross power density model

We fit our stack model to experimental results reported in the literature. The setup employed by Vermaas et al. [1] consists of a stack of Fumatech FKS (CEM) and FAS (AEM) membranes, each 10 cm long by 10 cm wide, with 100 μm diluate and concentrate channel heights and two electrodes. The inlet feed salinities are 29,120 ppm (30 g NaCl per kg water) concentrate and 1,000 ppm (1 g NaCl per kg water) diluate.

The fitted parameters were the salt transport number t_s, the Sherwood correlation coefficient K_m, and the spacer porosity ϵ. The salt and water permeability L_s and L_w were set to conventional values for electrodialysis (see Table 2.1).

In Fig. 2-7, we show the fit to the ohmic surface resistance $\bar{r}_{ohm}$ and in Fig. 2-8 we show the fit to the total equivalent stack surface resistance $\bar{r}_{eq}$. The ohmic surface resistance is the sum of the membrane surface resistances $\bar{r}_{\text{AEM}}$ and $\bar{r}_{\text{CEM}}$, the diluate channel surface resistance $\bar{r}_d$, and the concentrate channel surface resistance $\bar{r}_c$. The total equivalent stack surface resistance $\bar{r}_{eq}$ consists of the ohmic surface resistance $\bar{r}_{ohm}$ and losses due to concentration polarization and concentration variation along the stack:

$$\phi_{\text{stack}} = \varepsilon_i^* - \bar{r}_{eq} j_{D,tot} \tag{2.20}$$

where ε_i^* is the local EMF at the inlet without including concentration polarization. The total current density is determined from load resistance matching ($R_L = \bar{r}_{eq}/wl$).

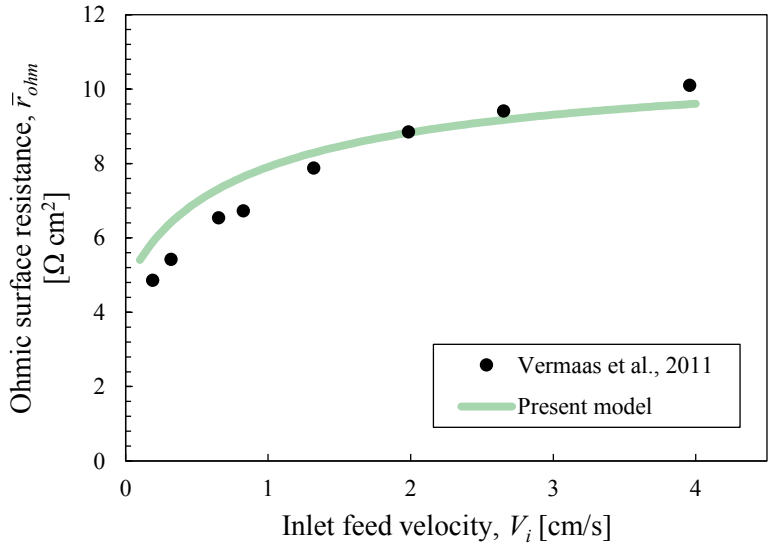

Figure 2-7: Validation of the model with respect to the ohmic surface resistance $\bar{r}_{ohm}$. The root mean squared error in the fit is 0.62 Ω cm^2.

The Sherwood correlation constant, K_m, is determined by fitting an equivalent stack resistance predicted by the model to the total stack resistance reported by Vermaas et al. The currents at which the equivalent stack resistances are computed are chosen by setting the load resistances equal to the equivalent stack resistances, as in traditional load matching. The results of the fit are shown in Fig. 2-8 below.

The power density predicted by the model is validated against the power densities reported by Vermaas et al. in Fig. 2-9 below.

2.2.7 Validation of the stack pumping power model

We model the pressure drop across the stack Δp as a laminar flow between two infinite plates, with a modifying constant K_p that accounts for the additional head loss caused by the spacers:

$$\Delta p = \frac{K_p \mu l V_i}{h_d^2} \tag{2.21}$$

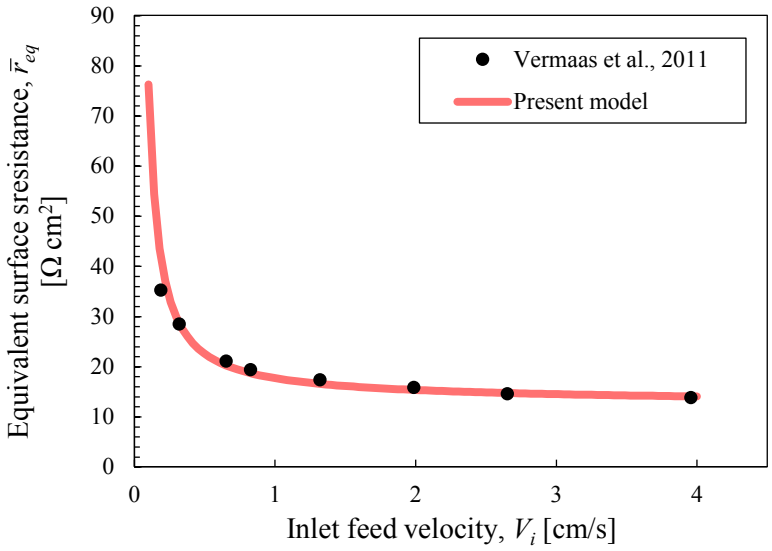

Figure 2-8: Validation of the model with respect to measured equivalent stack surface resistance at various flow rates. The root mean squared error in the fit is 4.7 Ω cm^2.

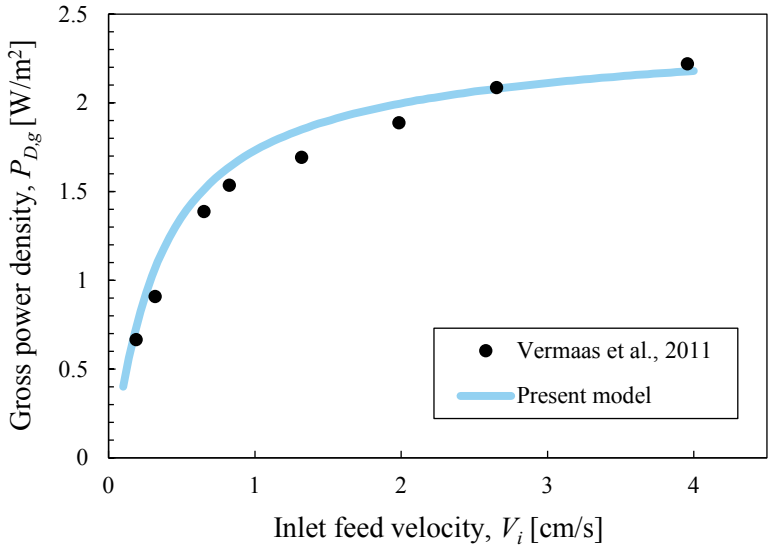

Figure 2-9: Validation of the model with respect to gross power densities reported by Vermaas at various flow rates. The root mean squared error in the fit is 0.085 W/m^2.

The constant K_p was determined by fitting the model to experimental results reported by Vermaas et al. [1], see Fig. 2-10 below. Multiplying by the flow rate and dividing by the active membrane area yields the stack pumping power density $P_{D,s}$ (Eq. 2.14).

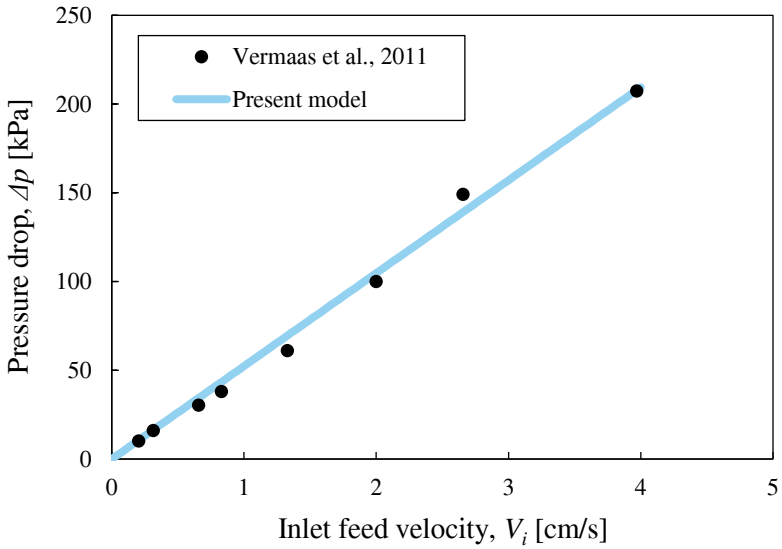

Figure 2-10: The model for the pressure drop across an RED stack with 100 μm channel heights is fit to experimental results reported by Vermaas et al. [1]. A constant K_p of 293 fits the data to within a maximum error of 14%.

2.2.8 Summary of the input model parameters

A summary of the model parameters and properties is provided in Table 2.1.

2.3 Dependence of power density and cost on load resistance

The load resistance which minimizes the levelized cost of electricity also maximizes the gross power density, because all other terms in the levelized cost (Eq. 2.19) and net power density are constant with respect to load resistance. The primary trade-off determining the cost-effective load resistance is therefore between a high stack voltage and high stack current. According to Eq. 2.8, the stack voltage increases with increasing load resistance. At the same time, the local stack currents $j_{D,n}$ decrease according to Eq. 2.5 - primarily because of the increase in stack voltage.

Figure 2-11 shows how the gross power density varies with a dimensionless load resistance $\Theta = R_L/R_{eq}$ holding all other parameters constant. R_{eq} is an equivalent total stack resistance

Table 2.1: Membrane, solution, channel and flow, as well as costing parameters and properties used in the analysis

Symbol	Value	Ref.
Membrane/Spacer Parameters		
$C_{d,i}$	1,000 ppm	-
$C_{c,i}$	35,000 ppm	-
ϵ	0.35	[22]
Γ	20 yrs	[29]
H^a	3.66 m	[29]
t_s	0.71	Sect. 2.2.6
t_w	10	[34]
L_s	1.4×10^{-8} m/s	[34]
L_w	1.4×10^{-5} mol/bar-m^2-s	[34]
$\bar{r}_{\mathrm{AEM}}$	1 Ω-cm^2	[22]
$\bar{r}_{\mathrm{CEM}}$	1 Ω-cm^2	[22]
r	6%	[29]
Solution Properties		
D_{NaCl}	1.61×10^{-9} m^2/s	[28]
μ	8.94×10^{-4} kg-m/s	[23]
Channel/Flow Parameters		
w	10 cm	[1]
h_c , h_d	100 μm	[1]
K_m	0.1	Sect. 2.2.6
K_p	293	Sect. 2.2.7
T	298 K	-
Cost Parameters		
K_{mem}	\$750/m^2	[24]
K_{PT}	\$20/(m^3/day)	[29, 31]

[a] Represents the average of the measured head losses by Post et al. [29] in the summer, winter, and spring

(technically defined as the Thévenin equivalent resistance of the circuit depicted in Fig. 2-4). At low Θ, large gains in stack voltage with increasing load resistance outweigh small reductions in stack current; the gross power density increases. Beyond the optimal Θ, the reductions in stack current outweigh the gains in stack voltage; the gross power density decreases.

Figure 2-12 shows how the levelized cost of electricity varies with dimensionless load

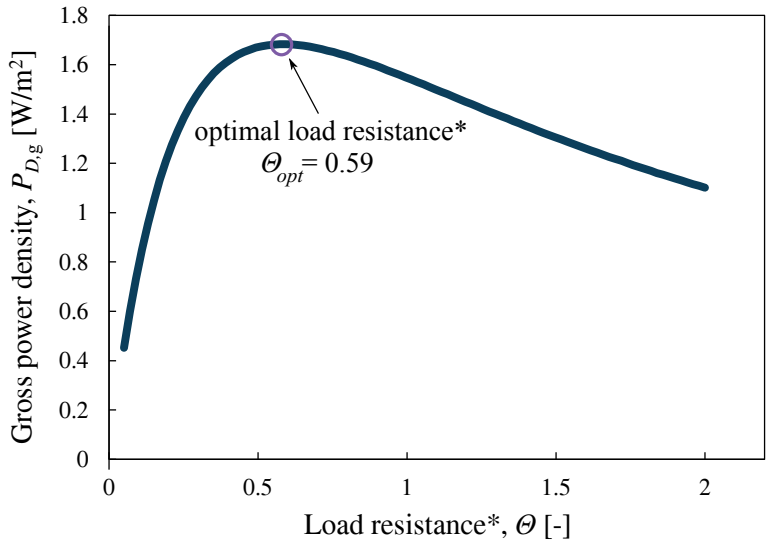

Figure 2-11: The load resistance which maximizes the gross power density is smaller than the equivalent stack resistance. The feed velocity and residence time are held constant at 0.5 cm/s and 20 s, respectively. The inlet diluate feed salinity is 1,000 ppm and the inlet concentrate feed salinity is 35,000 ppm.

resistance, confirming that the load resistance which maximizes the gross power density also minimizes the levelized cost of electricity. The optimal load resistance is 0.12 Ω per cell pair.

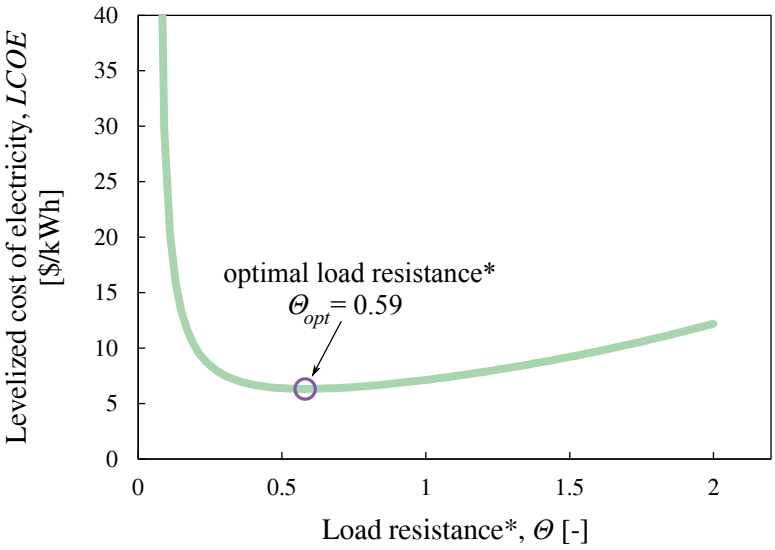

Figure 2-12: The load resistance which maximizes the gross power density also minimizes the levelized cost of electricity. The inlet diluate feed salinity is 1,000 ppm and the inlet concentrate feed salinity is 35,000 ppm.

Interestingly, Figs. 2-11 and 2-12 show that the optimal load resistance is *smaller* than the equivalent total stack resistance (i.e. $\Theta_{opt} < 1$). If traditional load matching were optimal, $\Theta_{opt} = 1$ would maximize the gross power density.

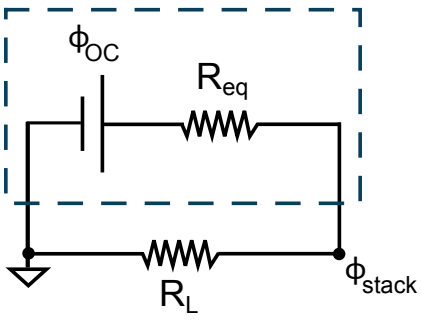

Figure 2-13: The circuit shown in Fig. 2-4 may be reduced to a Thévenin equivalent circuit defined by the open-circuit voltage ϕ_{OC} and an equivalent stack resistance R_{eq}. The equivalent stack resistance accounts for changes in the streamwise salinity profile along the stack, see Eq. 2.20.

We prove that the optimal load resistance is always smaller than the equivalent stack resistance - regardless of the feed velocity or residence time chosen - by considering the Thévenin equivalent circuit depicted in Figure 2-13. The gross power density may be expressed as:

$$P_{D,g} = \left(\frac{\phi_{OC}}{R_{eq} + R_L}\right)^2 \frac{R_L}{wl} \tag{2.22}$$

where ϕ_{OC} is the open-circuit voltage. When streamwise variations in concentration are accounted for, $R_{eq} = f(R_L)$, because changes in load resistance are coupled to changes in current and salt transport. Additionally, the open-circuit voltage is not a function of load resistance, because the load resistance is infinite in an open circuit. Maximizing the gross power density with respect to the load resistance R_L yields the following expression for the optimal load resistance $R_{L,opt}$:

$$R_{L,opt} = \frac{R_{eq}}{2\frac{\partial R_{eq}}{\partial R_L} + 1} \tag{2.23}$$

The sign of $\partial R_{eq}/\partial R_L$ is always positive, because as the load resistance increases, the total

current density decreases, reducing migrative ion transport to the diluate channel, reducing the average diluate conductivity. According to Eq. 2.7, this increases the diluate channel resistance, the dominant resistance in the equivalent stack resistance R_{eq}. Because $\partial R_{eq}/\partial R_L$ is always positive, the optimal load resistance is always smaller than the equivalent stack resistance. Choosing the optimal load resistance versus simply load matching reduces the levelized cost of electricity by more than 30%.

2.4 Step 1: Fix the residence time

Initially, we fix the residence time to 20 s before computing the optimal feed velocity. We fix the residence time first, as opposed to the feed velocity, because beyond a critical residence time τ_c costs are relatively insensitive to changes in residence time (see Fig. 2-14). The rapid fall in cost at low residence times is caused by a significant rise in the net power density. At low residence times, the large pretreatment pumping power density dominates the gross power density output of the stack, driving the net power density to zero (see Eq. 2.13). At larger residence times, the pretreatment pumping power density is small compared to the gross power density of the stack. Costs rise mildly, primarily because the gross power density decreases mildly with residence time. For this configuration, a residence time of 20 s is situated comfortably beyond the critical residence time for a wide range of velocities. We will return to this trade-off in Sect. 2.6.

2.5 Step 2: Optimize the velocity

With a fixed residence time, we minimize the levelized cost of electricity with respect to the inlet feed velocity V_i. Figure 2-15 shows the gross power density and pumping losses through the pretreatment system and stack when varying only the feed velocity. Figure 2-16 shows the resulting net power density. We find that a velocity of 0.46 cm/s minimizes the levelized cost of electricity for a typical seawater/river water configuration. The levelized cost of electricity is 6.33 $/kWh.

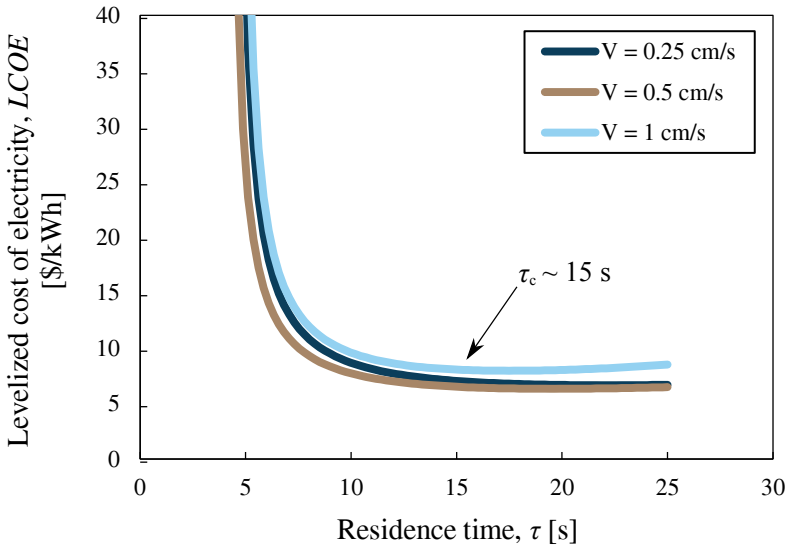

Figure 2-14: The dependence of levelized cost of electricity on residence time for a range of velocities.

Equation 2.19 shows that with a fixed residence time, the cost-effective feed velocity simply maximizes the net power density. The pumping power losses through the pretreatment system $P_{D,PT}$ (Eq. 2.13) and, to first order, the rate of salt transport are constant with velocity when residence time is fixed. Therefore the primary trade-off in determining the optimal feed velocity is between concentration polarization losses in the gross power density and pumping power losses through the stack.

At low velocities, the losses due to concentration polarization are highly non-linear. Marginal increases in feed velocity result in large gross power density gains which outweigh increased pumping losses through the stack; the net power density rises with increasing feed velocity. At high velocities, the gross power density gains level off as the concentration polarization losses approach linearity. Pumping power losses through the stack dominate, driving the net power density down. At the maximum net power density, the curvature of the plot is sufficiently small that velocities within 20% of the optimum reduce the net power density by less than 1%. With a fixed residence time, the levelized cost of electricity varies inversely with the net power density, see Fig. 2-17. Velocities within 20% of the optimum reduce the levelized cost of electricity by less than 1% as well.

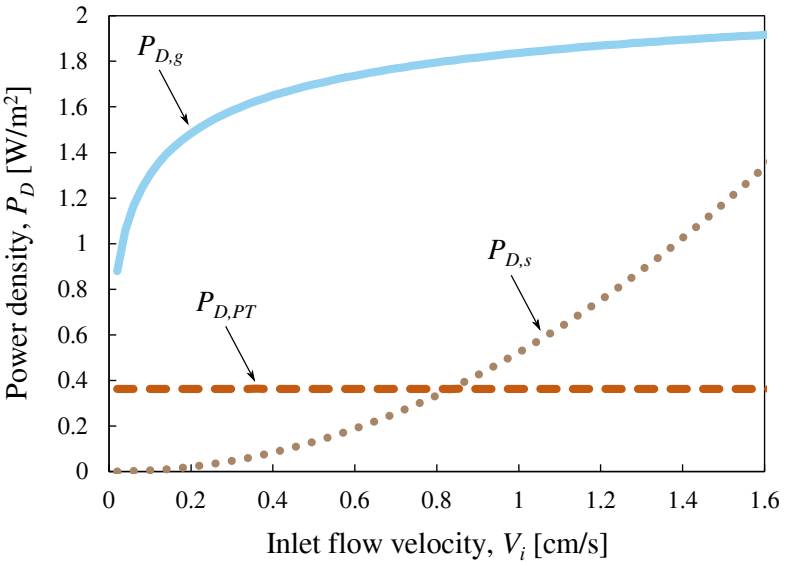

Figure 2-15: The residence time is fixed, and we vary the feed velocity. The gross power density $P_{D,g}$ and the power density consumed for pumping through the stack $P_{D,s}$ and pretreatment system $P_{D,PT}$ are shown.

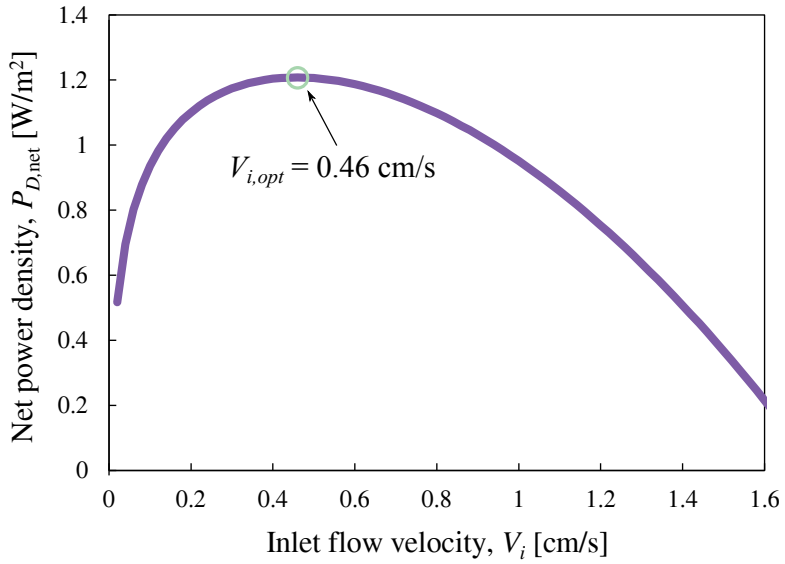

Figure 2-16: The residence time is fixed, and we vary the feed velocity. The net power density $P_{D,\text{net}}$ and the optimal feed velocity $V_{i,opt}$ are shown.

The optimal feed velocity is significantly smaller than what is proposed in the literature. For a 10 cm long stack, an optimal feed velocity of 1 cm/s was found [1]. The optimization procedure consisted of fixing the stack length and measuring the net power density (not

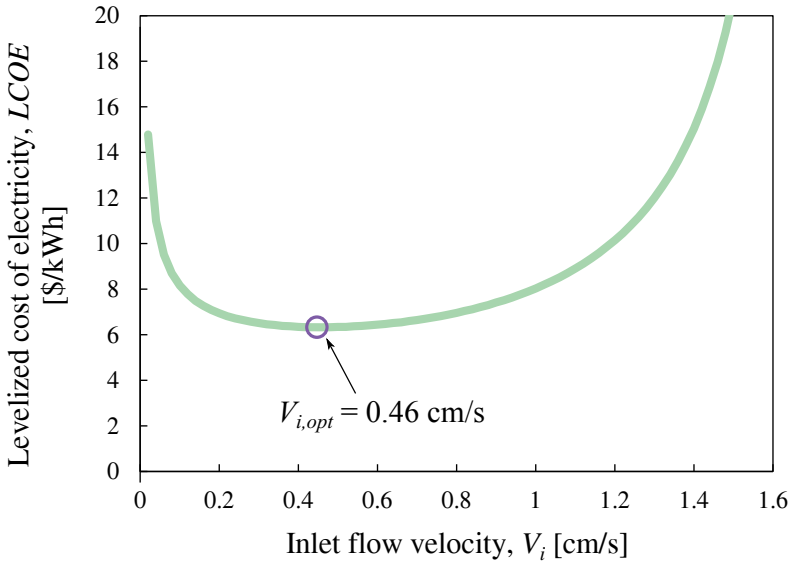

Figure 2-17: The residence time is fixed, and we vary the feed velocity. The levelized cost of electricity $LCOE$ and the optimal feed velocity $V_{i,opt}$ are shown.

including the required pumping power through the pretreatment system) for different feed velocities, as opposed to optimizing both length and velocity with respect to levelized cost.

2.6 Step 4: Optimize the residence time

The velocity is fixed to 0.46 cm/s, and we minimize the levelized cost of electricity with respect to residence time. Unlike the optimal velocity, the optimal residence time does not simply maximize the net power density. Instead, the optimal residence time balances a trade-off between both the stack and pretreatment capital costs (see Eq. 2.19). We find that a residence time of 19.9 s minimizes the levelized cost of electricity for the typical seawater/river water stack. With an optimal velocity of 0.46 cm/s, this corresponds to an optimal stack length of 9.2 cm. The levelized cost of electricity is 6.33 $/kWh.

Figure 2-18 shows how the gross power density and pumping losses through the pretreatment system and stack vary with residence time, and Fig. 2-19 shows the resulting net power density. The residence time which maximizes the net power density τ^* weighs the trade-off between the gross power density and the pretreatment pumping power. The gross power

density decreases with increasing residence time, because more salt is transported, reducing the average salinity gradient and local EMFs. On the other hand, pumping power density losses through the pretreatment system decrease with increasing residence time, because the losses are spread over a larger stack. A residence time of 19.7 s maximizes the net power density.

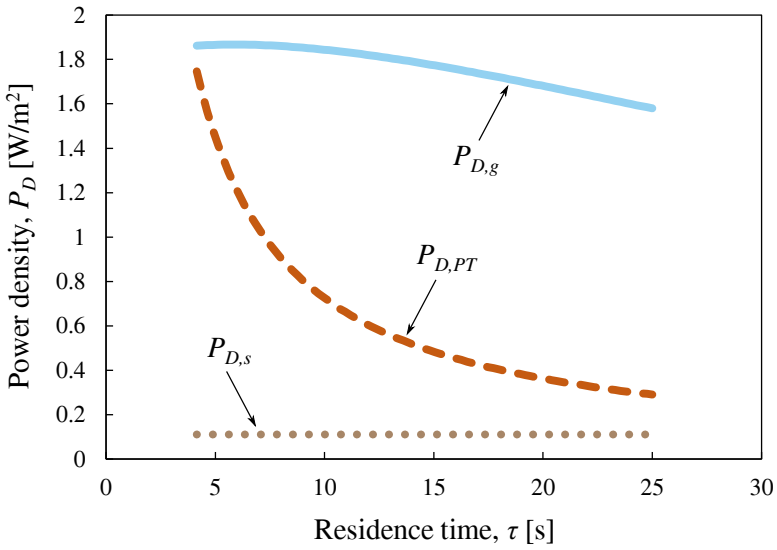

Figure 2-18: The velocity is fixed and the residence time is varied. The gross power density $P_{D,g}$ and the power density consumed for pumping through the stack $P_{D,s}$ and pretreatment system $P_{D,PT}$ are shown.

Figure 2-20 shows the levelized cost of electricity $LCOE$ with and without the pretreatment pumping power $P_{D,PT}$ considered. The optimal residence time τ_{opt} (with $P_{D,PT}$ considered) is 19.9 s. The optimal residence time τ_{opt} is larger than τ^*, because the pretreatment capital costs decrease with increasing residence time (see Eq. 2.19). When the pretreatment pumping power is considered, τ^* and τ_{opt} are both higher, because these losses are very costly at low residence times.

We compute an optimal residence time that is greater than what is found in the literature. The literature suggests an optimal residence time of 8 s for a similar stack configuration [22]. We find a longer residence time to be optimal, because we consider both pumping losses and capital costs associated with the pretreatment system. The large residence time results in an optimal stack length which is slightly smaller than what is currently advocated in the

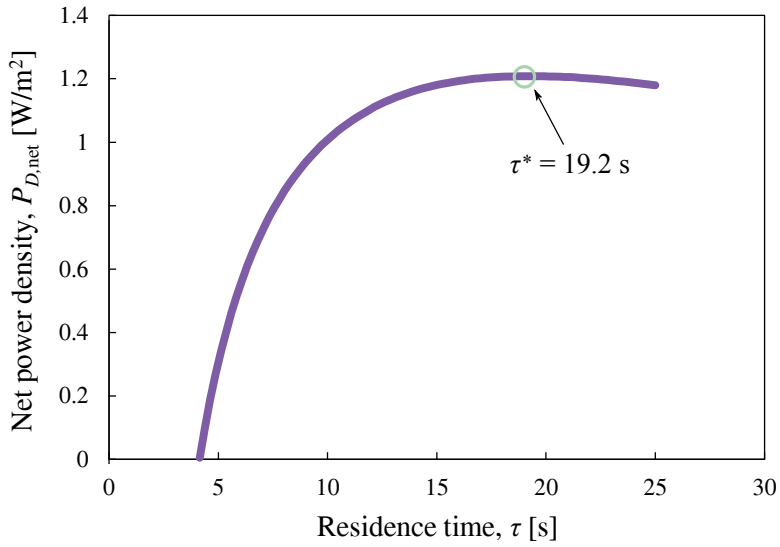

Figure 2-19: The velocity is fixed and the residence time is varied. The net power density $P_{D,\text{net}}$ and the residence time which maximizes the net power density τ^* are shown.

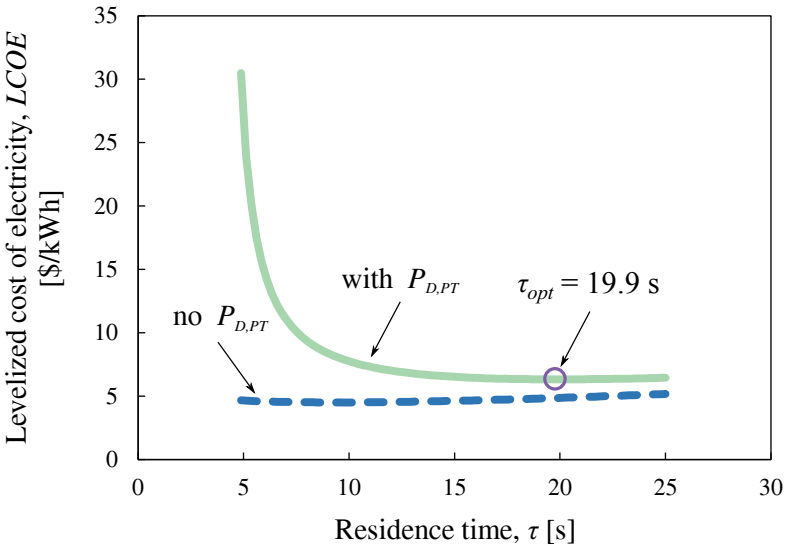

Figure 2-20: The velocity is fixed and the residence time is varied. We plot the levelized cost of electricity $LCOE$ with and without the pretreatment pumping power $P_{D,PT}$ considered. The optimal residence time τ_{opt} is larger than the one which maximizes the net power density τ^*.

literature. While on the face of it, the optimal stack length is only slightly different, this must be understood in the context of a significantly reduced feed velocity. The key insight is that more salt transport through the stack is optimal.

2.6.1 Sensitivity of the optimal residence time and optimal feed velocity to select parameters

We examine the sensitivity of the optimal residence time to the stack and pretreatment capital cost figures as well as the channel height by measuring the percent change in τ_{opt} resulting from a 1% decrease in each parameter. For example, as shown in Table 2.2, a 1% decrease in the stack capital cost parameter K_{mem} results in a 0.04% increase in the optimal residence time τ_{opt}.

Table 2.2: Sensitivity of residence time to cost parameters and channel height

Parameter	**Change in τ_{opt}**
K_{mem}	0.04%
K_{PT}	-0.03%
h	-1.4%

Of the three design parameters considered in this Chapter, the optimal residence time is the only one sensitive to cost parameters. As show in Table 2.2 the sensitivity is small. The optimal residence time is most sensitive to changes in the channel height.

The optimal feed velocity and optimal load resistance are also sensitive to changes in the channel height. We find that a 1% decrease in the channel height results in a -0.7% change in the optimal feed velocity and a -0.08% change in the optimal load resistance.

2.7 Cost comparison to other design strategies

We model the levelized cost of electricity associated with different design strategies found in the literature and compare the results in Fig. 2-21. The costs shown are significantly higher than those generally reported in the RED literature, primarily because we use a larger stack capital cost figure which is based on average electrodialysis stack costs deployed commercially. More importantly, however, the design strategy presented in this study results in a more than 40% reduction in the levelized cost of electricity as compared to the leading strategy in the literature, where $P_{D,g} - P_{D,s}$ (the net power density not including the pretreatment pumping

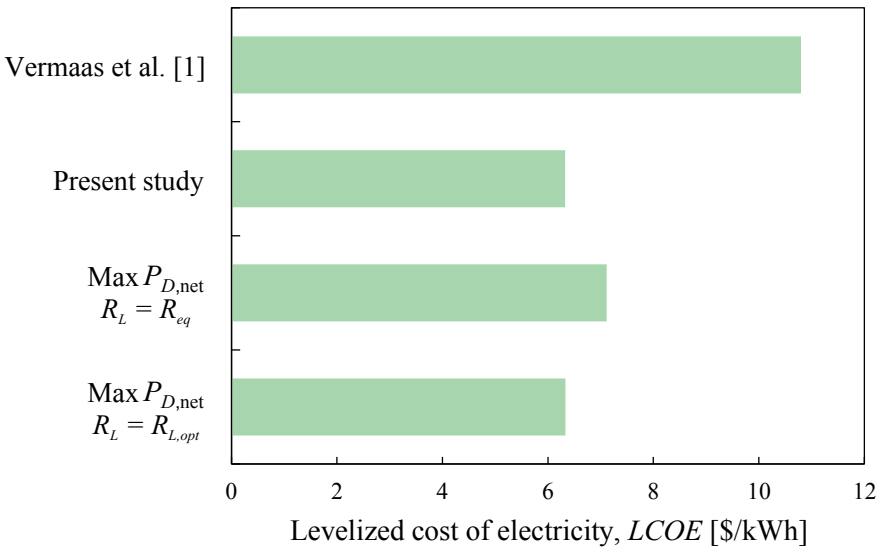

Figure 2-21: A cost comparison of different RED design strategies. The costs associated with design strategies where the gross power density is maximized or the response product is maximized were also modeled. Neither strategy resulted in a positive net power density output when pretreatment pumping power consumption was included.

power density) is maximized with respect to feed velocity and load resistance matching is employed [1]. No other strategy from the literature which we modeled, including maximizing the gross stack power density or maximizing the response product [18], resulted in a positive net power density output after pretreatment pumping power consumption was considered.

As an approximation to the strategy of minimizing the levelized cost of electricity, we consider maximizing the net power density in a form that includes the pumping power required to drive flow through the stack *and* the pretreatment system. For the range of cost parameters we considered, this approximate approach is accurate to within 0.1%. This accuracy arises because the capital cost per unit net power produced dominates the levelized cost of electricity. We expect the accuracy to diminish as the capital cost per unit net power produced decreases relative to the pretreatment cost per unit net power produced.

As a further approximation, we maximize this net power density with load matching ($R_L = R_{eq}$) instead of load optimization ($R_L = R_{L,opt}$). We find this to be an inferior method, as the resulting levelized cost of electricity is over 12% higher than our proposed approach. Nevertheless, even after employing our proposed design approach the levelized cost

of electricity remains nearly two orders of magnitude higher than current average electricity prices in the United States.

2.8 Conclusions

An optimal stack design based on the minimization of the levelized cost of electricity produced consists of a slightly shorter length, lower operating velocity, and smaller load resistance than is currently described in the literature. We prescribe a stack length of 9.2 cm, an operating velocity of 0.46 cm/s, and a load resistance of 0.12 Ω per cell pair for the typical seawater/freshwater system. Though costs remain high relative to other renewable technologies, these design implementations can reduce the levelized cost of electricity by over 40% compared to designs currently proposed in the literature.

THIS PAGE INTENTIONALLY LEFT BLANK

Chapter 3

Increasing the power density and reducing the levelized cost of electricity of a reverse electrodialysis stack through blending

Summary

In this chapter [1], we increase the power density of a reverse electrodialysis (RED) stack by blending the low salinity feed with a higher salinity stream before the stack entrance. This lowers the capital cost of the system, enhancing the viability of RED renewable energy production. Blending increases the power density by decreasing the dominating electrical resistance in the diluate channel as well as the effective resistance caused by concentration polarization, but not without sacrificing some driving potential. To quantify this trade-off and to evaluate the power density improvement blending can provide, a one-dimensional RED stack model is employed, validated with experimental results from the literature. For a typical stack configured with a feed velocity of 1 cm/s, power density improvements of over 20% and levelized cost of energy reductions of over 40% are achievable, provided the

[1] The author acknowledges contributions from Ronan McGovern to the work in this chapter

salinity of the available river water is below 200 ppm. Additional cost reductions are realized through back-end blending, whereby the diluate exit stream is used as the higher salinity feed. Additionally, improvements from blending increase for higher feed velocities, shorter stack lengths, and larger channel heights.

3.1 Introduction

The objective of this chapter is to quantify the viability of blending as a design approach for improving the power density of future RED stacks installed at promising locations around the world. An examination of these locations suggests that salinity gradient power production through reverse electrodialysis (RED) could potentially provide 1 TW of clean, uninterrupted power globally [29]. However, the future competitiveness of RED as a renewable energy technology will depend upon the achievement of significant reductions in capital cost, through lower membrane prices and higher power densities [16].

As shown in a recent study of the financial feasibility of reverse electrodialysis [16], capital cost - driven by the gross power density of the stack - is the dominant contributor to the levelized cost of electricity produced by RED. Thus, raising the power density represents the greatest potential for enhancing RED viability.

One effective method for raising the power density is by reducing the electrical resistance through the stack. As evidenced by Fig. 3-1, significant improvements may be made by reducing the dominant diluate or low conductivity stream resistance $\bar{r}_d$. This reduction may be accomplished in any of the following three ways: by reducing the height of the diluate channel; by reducing the spacer shadow effect; or by increasing the diluate conductivity through blending a high salinity stream with the river water feed [35]. Both reducing the diluate channel height and reducing the spacer shadow effect have been studied extensively in the literature and can significantly improve the power density [1, 20, 21]. However, neither method is free from trade-offs. Reducing the diluate channel height increases the required pumping power [1], which lowers the net power density; such reduction may also be limited by manufacturing considerations. Similarly, reducing the spacer shadow effect increases the

effective concentration polarization resistance [20].

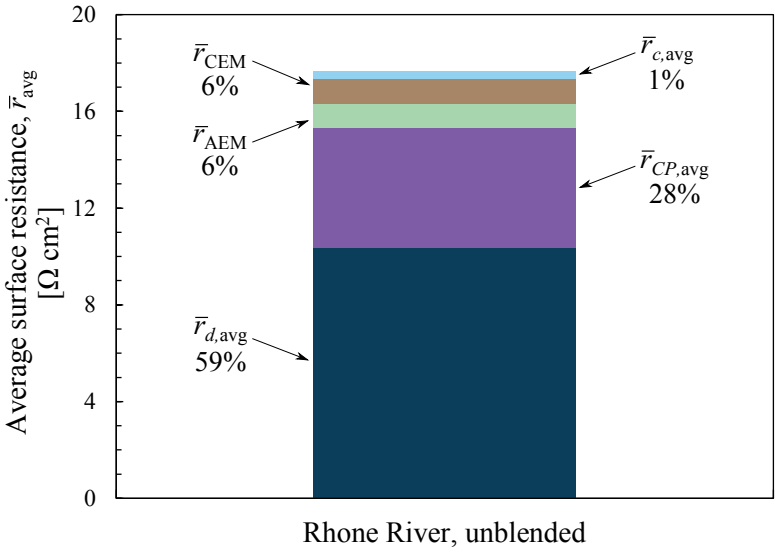

Figure 3-1: Total resistive losses through a typical RED stack include contributions from the concentrate channel $\bar{r}_c$, anion and cation exchange membranes $\bar{r}_{\mathrm{AEM}}$ and $\bar{r}_{\mathrm{CEM}}$, effect of concentration polarization $\bar{r}_{\mathrm{CP}}$, as well as from the diluate channel $\bar{r}_d$. Reduction of the diluate channel and effective concentration polarization surface resistances holds the greatest potential for improving RED power density. The case shown assumes a diluate feed from the Rhone River (339 ppm salinity [2]), a channel height of 100 μm, stack length of 10 cm, and feed velocity of 1 cm/s. Here, each contributing surface resistance is averaged over the RED length.

Although raising the diluate conductivity through blending has its own set of trade-offs, it significantly reduces both the diluate and effective concentration polarization surface resistances, and should be given careful consideration. With blending, a fundamental trade-off is made between minimizing the diluate resistance and maximizing the driving potential for charge transport by optimizing the diluate salinity. As shown in Fig. 3-2, by blending a portion of the higher salinity stream with the river water before the RED stack entrance, the salinity of the river water may be increased. Optimization of the amount of blending allows the power density of the stack to be maximized.

Currently, there are many studies in the literature illustrating the trade-off between diluate resistance and driving potential, but there are no studies devoted to quantifying the power density gains made through blending. Weinstein and Leitz [36] and Lacey [37]

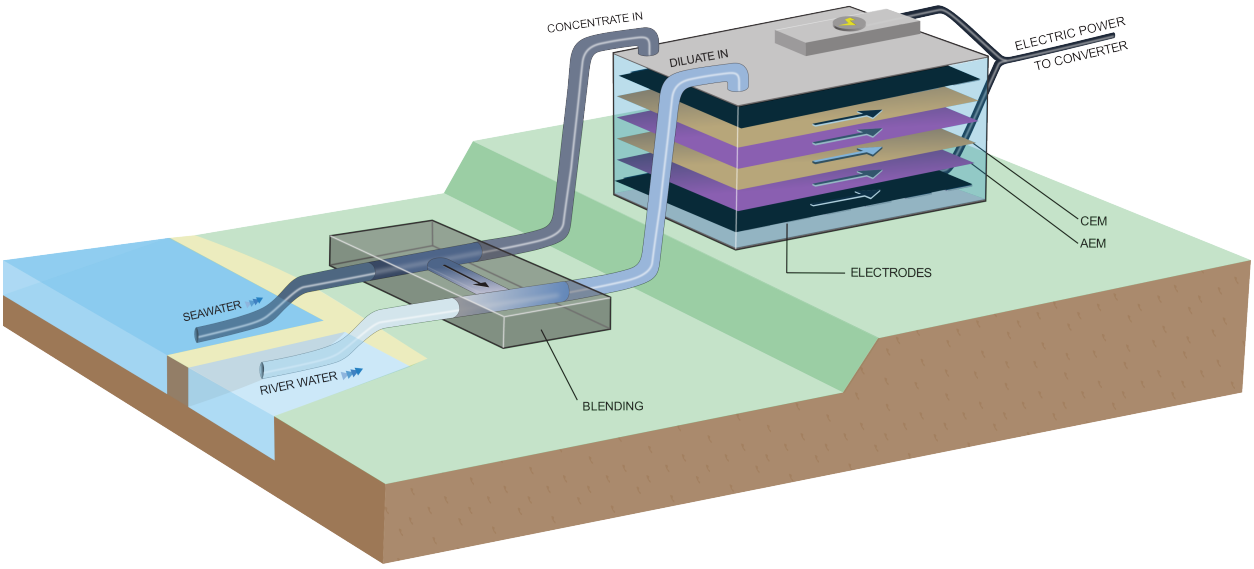

Figure 3-2: One embodiment of blending (front-end blending) involves the continuous withdrawal of pretreated river water and seawater and the continuous blending of a portion of the seawater with the river water before feeding the streams to the stack concentrate and diluate inlets.

modeled and computed the optimal diluate concentration in a zero-dimensional RED stack (a stack of infinitesimal length) with a seawater concentrate stream. Similarly, Veerman et al. [18] showed that the local power density in a one-dimensional stack (a stack of finite length) initially increases and reaches a maximum with respect to increasing local diluate concentration within the stack. The same trade-off is found in using electrodialysis for desalination. McGovern et al. [32, 38] showed that removing salt from higher diluate salinity feeds significantly reduces the capital cost, because the resistance is lower.

Other studies have examined different feed waters for salinity gradient power generation, but none have considered blending the feed water as a design approach [14, 16, 39]. As an example, Daniilidis et al. [16] experimentally investigated RED power density and efficiency across a wide range of feed water salinities beyond river and seawater applications showing that power density continues to increase at very large salinity gradients despite reductions in permselectivity.

In a 2009 study of the various power output limitations in an RED stack, Dlugolecki et al. [35] mentioned blending as a possible means for reducing the resistance of the diluate

channel, without specifically quantifying the potential power density improvements. The study cites early RED work by Weinstein and Leitz [36] from whose results it may be inferred that blending 600 ppm river water with seawater in a stack of infinitesimal length (which does not account for streamwise variations in concentration as the diluate and concentrate travel through the RED channels) could improve RED power density by upwards of 30%. Since Weinstein and Leitz's zero-dimensional study, significant advancements have been made in improving RED technology and stack design and in understanding and modeling the loss mechanisms as well. Absent from the current literature is a quantification of blending improvements since this progress.

In this chapter, we analyze the viability of blending in the context of the current modeling methods. First, we analyze blending using a one-dimensional model which accounts for streamwise variations in salinity. In Sect. 3.4.2, we show that, when inflowing river water is at 600 ppm, blending results in a minimal power density gain. Second, we analyze blending using a model which includes concentration polarization effects. We show in Sect. 3.5.1 that blending also reduces the effective concentration polarization resistance.

We also analyze the viability of blending in the context of recent designs. As an example, RED membrane resistances have decreased by over 90% since early RED development and no longer dominate resistive losses (see Fig. 3-1). Additionally, channel heights have decreased ten-fold. We then extend the study by quantifying how blending may impact future stack configurations (see Sect. 3.5.3), concluding that improvements increase with shorter residence times and larger channel heights.

Lastly, we propose and analyze a blending configuration in which the diluate feed is recycled, see Fig. 3-3. In this configuration (termed back-end blending with diluate recirculation), recycling of the diluate feed reduces pretreatment system capital, operating, and energy costs - an additional benefit. We briefly analyze and discuss the cost advantages over front-end blending in Sect. 3.4.3.

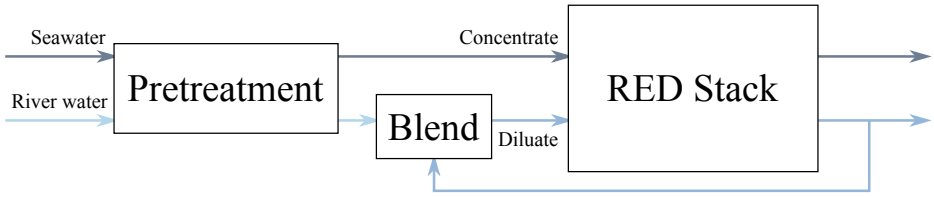

Figure 3-3: Back-end blending with diluate recirculation. The advantages are reductions in pretreatment capital, operating, and energy costs.

3.2 Methods

To quantify the gross power density improvements achieved through blending, we model a single-cell RED stack accounting for salinity variations in the streamwise direction. We model three stack designs proposed in the literature, each characterized by different feed velocities - 0.5 cm/s (from Chapter 2), 1 cm/s [1], and 1.25 cm/s [22]. All three designs have 100 μm channel heights and 10 cm stack lengths. For each design, we maximize the gross power density with respect to the load resistance and inlet diluate salinity. We then compare this power density to the power density achieved with unblended river water (with the load resistance optimized) to evaluate the gross power density improvement.

To quantify the cost advantages of back-end blending over front-end blending, we model the RED net power density and levelized cost of electricity for the front-end and back-end blending cases, noting that for fixed velocities, the pumping power will be the same. As in the gross power density case, we repeat this analysis for three different feed velocities, keeping the stack length fixed.

3.2.1 Gross power density model

The RED gross power density model is based on the approach taken in Chapter 2. As in Chapter 2, we fix the diluate and concentrate channel heights h and set them equal, as well as set the diluate and concentrate inlet feed velocities V_i equal. This simplifies the stack design. Figure 3-4 shows the cell pair circuit diagram, which is divided into N discrete segments for modeling stream-wise variations in electromotive force (EMF) ε_n, diluate resistance $\bar{r}_{d,n}$, and

concentrate resistance $\bar{r}_{c,n}$. The variations result from changes in salinity along the length due to salt and water transport across the membranes. We neglect variations in membrane resistance as well as the existence of ionic shortcut currents [40]. The model is validated as in Chapter 2.

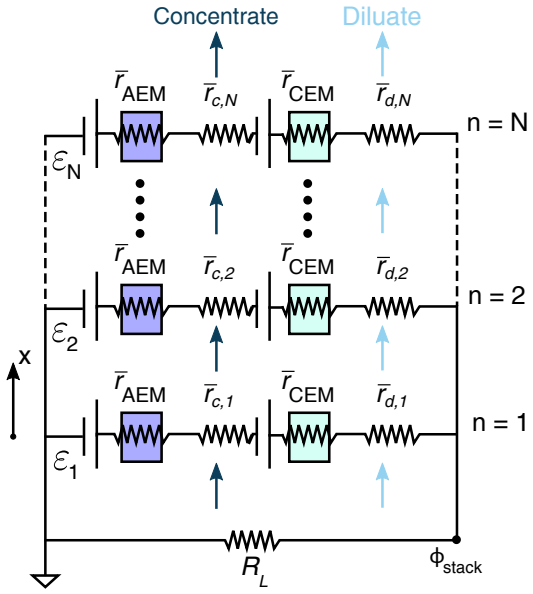

Figure 3-4: A circuit model for the one-dimensional, unsegmented-electrode RED stack which accounts for streamwise variations in salinity.

The local EMFs ε_n are computed from the local chemical potential differences across the membranes [30]:

$$\varepsilon_n = \frac{t_s}{F}\left(\mu^s_{c,n} - \mu^s_{d,n}\right) + \frac{t_w}{F}\left(\mu^w_{c,n} - \mu^w_{d,n}\right) \tag{3.1}$$

where t_s is the salt transport number, t_w is the water transport number, F is Faraday's constant, $\mu^s_{c,n}$ is the local salt chemical potential at the membrane surface on the concentrate side, and $\mu^s_{d,n}$ is the local salt chemical potential at the membrane surface on the diluate side. Blending reduces the difference between $\mu^s_{c,n}$ and $\mu^s_{d,n}$, driving the local EMFs down. This detrimental effect is a trade-off against reduced stack resistance brought about by the increased diluate salinity.

We model concentration polarization using a convection-diffusion approach [11] (diluate

example shown):

$$C_{d,m,n} - C_{d,n} = \frac{2h}{\mathrm{Sh}_{d,n}} \frac{j_{D,n}}{F} \frac{(\bar{T}_{cu} - t_{cu})}{D_{\mathrm{NaCl}}} \tag{3.2}$$

where $C_{d,m,n}$ is the local diluate concentration at the membrane (an input to $\mu^s_{d,n}$), $C_{d,n}$ is the local diluate concentration in the bulk, $j_{D,n}$ is the local current density (see Eq. 3.11 below), h is the channel height, t_{cu} is the counter-ion transport number ($\approx$0.5 for anions and cations), and D_{NaCl} is the diffusion coefficient of salt through the bulk. $\bar{T}_{cu}$ is the integral counter-ion transport number [24]:

$$\bar{T}_{cu} \approx \frac{t_s + 1}{2} \tag{3.3}$$

$\mathrm{Sh}_{d,n}$ is the local Sherwood number [25] (diluate example shown):

$$\mathrm{Sh}_{d,n} = K_m \mathrm{Re}^{1/2}_{D_h,d,n} \mathrm{Sc}^{1/3}_{d,n} \tag{3.4}$$

where K_m is the Kuroda constant, $\mathrm{Re}_{D_h,d,n}$ is the local Reynolds number based on the hydraulic diameter D_h, and $\mathrm{Sc}_{d,n}$ is the local Schmidt number.

When the difference in concentration between the bulk and membrane is small compared to the diluate concentration, one can approximate concentration polarization as a linearized ohmic surface resistance. Concentration polarization reduces the local EMFs in RED by increasing the salt concentration at the membrane wall in the diluate channel, while decreasing the concentration at the membrane wall on the concentrate side. The reduction in local EMF may be linearized and rewritten as an effective local ohmic resistance by first expanding out the local EMF (Eq. 3.1) using the Nernst equation:

$$\varepsilon_n = t_s \frac{RT}{F} \ln \frac{\gamma_c C_{c,m,n}}{\gamma_d C_{d,m,n}} \tag{3.5}$$

where T is the temperature, and γ_c and γ_d are the activity coefficients of the concentrate and diluate (as modeled by Pitzer [41]). Assuming the concentration difference between the membrane and bulk $|\Delta C_n|$ is the same in either channel, the local EMF may be rewritten

as:

$$\varepsilon_n = t_s \frac{RT}{F} \ln \frac{\gamma_c C_{c,n}(1 - |\Delta C_n|/C_{c,n})}{\gamma_d C_{d,n}(1 + |\Delta C_n|/C_{d,n})} \tag{3.6}$$

Equation 3.6 may be separated and Taylor expanded, and if $|\Delta C_n|/C_{d,n}$ is small (which generally holds), may be simplified into the sum of a regular Nernst potential and a concentration polarization potential loss term:

$$\varepsilon_n = t_s \frac{RT}{F} \left[\ln \frac{\gamma_c C_{c,n}}{\gamma_d C_{d,n}} - \Delta C_n \left(\frac{1}{C_{c,n}} + \frac{1}{C_{d,n}} \right) \right] \tag{3.7}$$

where the concentration change ΔC_n is given by Eq. 3.2.

Substituting Eq. 3.2 into Eq. 3.7, reveals a concentration polarization potential loss which is linear with local current density $j_{D,n}$. The effective concentration polarization surface resistance may therefore be defined as:

$$\bar{r}_{\mathrm{CP},n} = \frac{2 t_s h RT}{F^2 \mathrm{Sh}_{d,n}} \frac{(\bar{T}_{cu} - t_{cu})}{D_{NaCl}} \left(\frac{1}{C_{c,n}} + \frac{1}{C_{d,n}} \right) \tag{3.8}$$

Equation 3.8 reveals that increased blending (and by extension, increased $C_{d,n}$) drives this effective concentration polarization resistance lower.

The other resistance sources are combined in the total ohmic surface resistance $\bar{r}_{tot,n}$ [22]:

$$\bar{r}_{tot,n} = \bar{r}_{\mathrm{AEM}} + \bar{r}_{\mathrm{CEM}} + \bar{r}_{d,n} + \bar{r}_{c,n} \tag{3.9}$$

Membrane resistances $\bar{r}_{\mathrm{AEM}}$ and $\bar{r}_{\mathrm{CEM}}$ generally decrease with increasing salinity (and therefore blending) [21], but they represent a small fraction of the total stack resistance. Consequently, we neglect any such variations.

The main benefit of blending is a reduction in the diluate resistance. The local diluate channel resistance $\bar{r}_{d,n}$ is modeled as [22]:

$$\bar{r}_{d,n} = \frac{h}{\epsilon^2 \kappa_{d,n}} \tag{3.10}$$

where ϵ is the spacer porosity and $\kappa_{d,n}$ is the diluate conductivity - the product of diluate

concentration $C_{d,n}$ and solution molar conductance $\Lambda_{d,n}$ [26]. The increase in conductivity with $C_{d,n}$ is slightly less than linear, as solution molar conductance $\Lambda_{d,n}$ decreases with concentration (see Fig. 3-5).

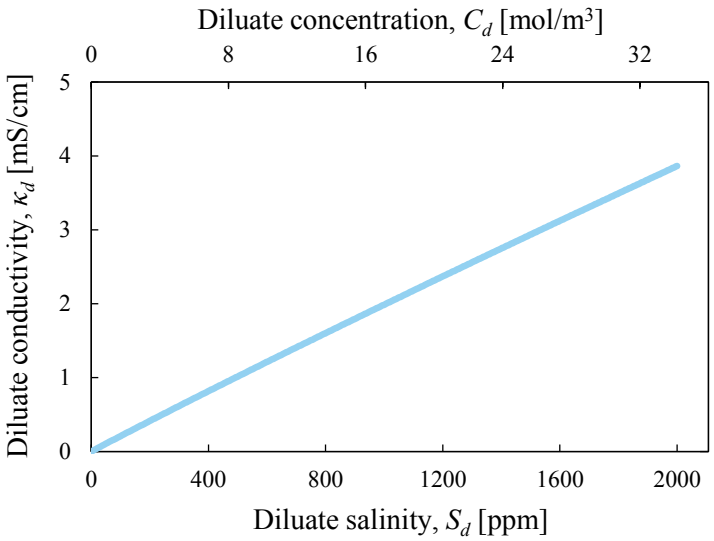

Figure 3-5: Diluate conductivity κ_d as a function of concentration, c_d, or salinity, S_d.

The local concentrate channel resistance $\bar{r}_{c,n}$ is modeled analogously to the diluate resistance although the impact of blending on this resistance is negligible.

Combining the local EMFs and resistance sources, provides the local current density:

$$j_{D,n} = \frac{\varepsilon_n - \phi_{\text{stack}}}{\bar{r}_{tot,n}} \tag{3.11}$$

where ϕ_{stack} is the total stack voltage. The total stack voltage is derived from Kirchoff's Current Law:

$$\phi_{\text{stack}} = \frac{\sum \frac{\varepsilon_n}{\bar{r}_{tot,n}} A_n}{\frac{1}{R_L} + \sum \frac{1}{\bar{r}_{tot,n}} A_n} \tag{3.12}$$

where A_n is the area of a segment and R_L is the load resistance.

The local molar salt and water fluxes $J_{s,n}$ and $J_{w,n}$ transported into the diluate channel

are modeled as in Fidaleo and Moresi [27]:

$$J_{s,n} = t_s \frac{j_{D,n}}{F} + L_s(C_{c,m,n} - C_{d,m,n}) \tag{3.13}$$

$$J_{w,n} = t_w \frac{j_{D,n}}{F} - L_w(\pi_{c,m,n} - \pi_{d,m,n}) \tag{3.14}$$

where L_s is the overall salt permeability (in m/s), L_w is the overall water permeability (in mol/bar-m^2-s), and $\pi_{m,n}$ is the local osmotic pressure at the membrane surface [28]. Finally, the gross power density $P_{D,g}$ is given by:

$$P_{D,g} = \frac{\phi_{\text{stack}}^2}{R_L w l} \tag{3.15}$$

where w is the stack width and l is the stack length. In our analysis, the load resistance R_L is continuously optimized with respect to the gross power density, as in Chapter 2.

3.2.2 Net power density model

The net power density $P_{D,\text{net}}$ is modeled as the gross power density less the stack pumping power density $P_{D,s}$ and the pumping power required through the pretreatment system $P_{D,PT}$, as in Chapter 2. The stack pumping power density is modeled as:

$$P_{D,s} = \frac{K_p \mu V_i^2}{h} \tag{3.16}$$

where K_p is a fitted parameter (accounting for the diluate and concentrate feeds) and μ is the feed viscosity. The stack pumping power model was fit to experimental data reported by Vermaas et al. [1]. The pretreatment system is modeled after a setup implemented by Post et al. [29], featuring coarse-media filtration with two drum filters. The required pumping power density through the system $P_{D,PT}$ is modeled as:

$$P_{D,PT} = [\rho_r(1 - X_{\text{blend}}) + \rho_c]\frac{gHh}{\tau} \tag{3.17}$$

where ρ is the feed density, X_{blend} is the mass fraction of exiting diluate diverted for blending, g is the gravitational body acceleration, H is the system head loss, and τ is the residence time (stack length divided by feed velocity). Equation 3.17 shows how back-end blending reduces the pumping power density required for pretreatment.

3.2.3 Modified cost model

When back-end blending as opposed to front-end blending is implemented, additional cost reductions are realized from recycling a portion of the already-pretreated diluate stream. To assess the impact of back-end blending on the levelized cost of electricity, we model the LCOE as in Chapter 2, with a slight modification to account for this recirculation:

$$LCOE = \frac{1}{P_{D,\text{net}}} \left[\frac{K_{mem}}{\text{CAF}} + (2 - X_{\text{blend}}) \frac{K_{PT} h}{\tau \text{CAF}} \right] \tag{3.18}$$

where K_{mem} is the RED stack capital cost figure in \$/m^2, K_{PT} is the pretreatment system capital cost figure in \$/(m^3/day), and CAF is the capital amortization factor [24]:

$$\text{CAF} = \frac{1}{r} \left[1 - \left(\frac{1}{1+r} \right)^{\Gamma} \right] \tag{3.19}$$

We assume a plant life Γ of 20 periods (one period is one year) and an annualized cost of capital r of 6% [29].

The constants used throughout the model are compiled in Sect. 3.3. To determine the salt and water permeabilities, salt transport number, and Kuroda constant, the model was fit to experimental data [1] (and shown in Chapter 2). All equations were solved using the quadratic approximation method in Engineering Equation Solver [23].

3.3 Summary of the input model parameters

A summary of the model parameters and equations is provided in Table 3.1

Table 3.1: Membrane, solution, channel and flow, as well as costing parameters and properties used in the analysis

Symbol	Value	Ref.
Membrane/Spacer Parameters		
$C_{c,i}$	35,000 ppm	-
ϵ	0.35	[22]
Γ	20	[29]
H^a	3.66 m	[29]
t_s	0.71	Sect. 2.2.6
t_w	10	[34]
t_{cu}	0.5	[24]
L_s	1.4×10^{-8} m/s	[34]
L_w	1.4×10^{-4} mol/bar-m^2-s	[34]
$\bar{r}_{\text{AEM}}$	1 Ω-cm^2	[22]
$\bar{r}_{\text{CEM}}$	1 Ω-cm^2	[22]
r	6%	[29]
Solution Properties		
D_{NaCl}	1.61×10^{-9} m^2/s	[28]
μ	8.94×10^{-4} kg-m/s	[23]
Channel/Flow Parameters		
w	10 cm	[1]
h_c , h_d	100 μm	[1]
K_m	0.1	Sect. 2.2.6
K_p	293	Sect. 2.2.7
T	298 K	-
Cost Parameters		
K_{mem}	\$750/m^2	[24]
$K_{PT}{}^b$	\$20/(m^3/day)	[29]

[a] Represents the average of the measured head losses by Post et al. [29] in the summer, winter, and spring
[b] Includes estimated operating (chemical) costs associated with pretreatment

3.4 Results

3.4.1 The optimal inlet diluate salinity

Figure 3-6 shows the computed inlet diluate salinity which maximizes the gross power density for the three RED stack designs. At salinities below the optimum, a net marginal benefit

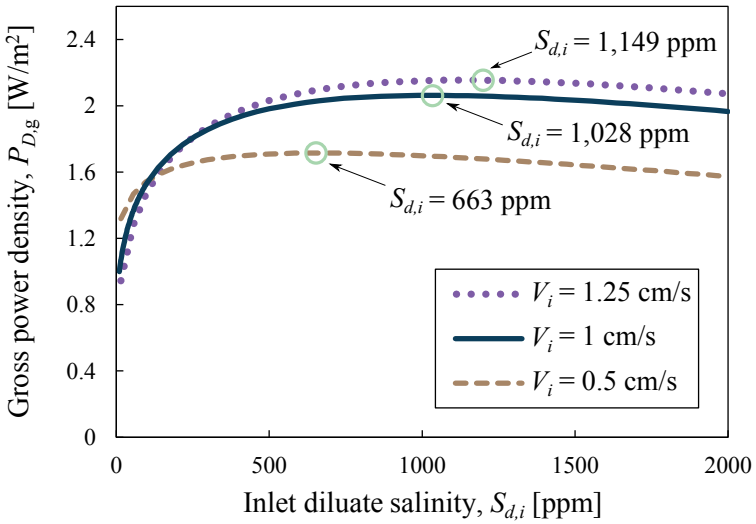

Figure 3-6: The inlet diluate salinity which maximizes the gross power density of an RED stack for three RED systems proposed in the literature

may be obtained by sacrificing some local driving potential to reduce stack resistance. At higher salinities, the marginal loss of driving potential exceeds the marginal gain from further reductions in diluate channel resistance and effective concentration polarization resistance.

The optimum inlet diluate salinity increases with feed velocity primarily as a result of decreasing salt transport along the stack. The reduced salt transport results in a lower average diluate salinity along the stack and thus a higher average driving potential, but also greater diluate resistance losses. Sacrificing some of the increased driving potential to reduce the diluate resistance by blending improves the overall power density.

For the RED stack with a length of 10 cm and a feed velocity of 0.5 cm/s, the optimal inlet diluate salinity is 663 ppm with a gross power density output of 1.72 W/m^2. Consequently, for this stack design blending improves the power density only if river water is available at a salinity below 663 ppm. Interestingly, all 8 major river mouth systems which Alvarez-Silva et al. [14] identified as suitable or partially suitable for salinity gradient power have average salinities below 663 ppm [2].

3.4.2 Power density improvements through blending

Figure 3-7 quantifies how the gross power density improvement varies with the available river water salinity up to 600 ppm. For the Rhone River (339 ppm), blending can improve the gross power density of the stack (with a feed velocity of 1 cm/s) by over 9%.

The gross power density improvement increases significantly at low river water salinities, primarily because the diluate resistance and effective concentration polarization resistance are proportional to the inverse of the diluate concentration (see Eqs. 3.8 and 3.10). The gross power density improvements approach infinity for a pure river water feed (0 ppm), because no power may be generated without blending.

Figure 3-8 shows the resulting percent reduction in the levelized cost of electricity by simply employing front-end blending. In the Rhone River case, cost reductions of over 21% are achievable.

For each feed velocity, there is a small but finite river water salinity at which, without blending, the gross power density is too low for the system to produce a positive net power density and the levelized cost of electricity approaches infinity. Consequently, there is a sharp rise in cost reductions brought about by blending for low salinity river water feeds. At higher salinity river water feeds, the cost reductions from blending diminish rapidly as gross power density improvements diminish.

3.4.3 Back-end vs. front-end blending

Figure 3-9 compares the total percent reduction in the levelized cost of electricity by employing front-end blending to the total percent reduction in cost by employing back-end blending with diluate recirculation. For all feed velocities and across all river water salinities, back-end blending offers additional cost reductions. These reductions are primarily due to the drop in the required pretreatment pumping power density which increases the net power density (see Eq. 3.17). Pretreatment capital and operating costs drop as well.

At low river water salinities, back-end improvements approach front-end improvements as the net power density approaches zero and reductions using either a back-end or front-end

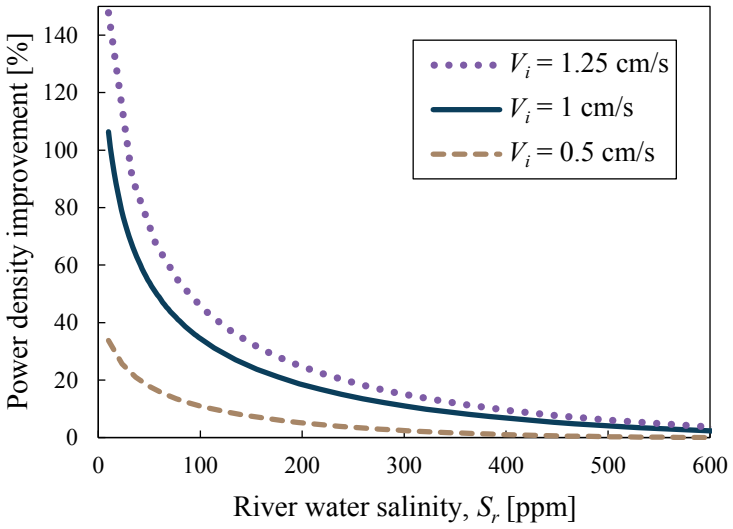

Figure 3-7: The percent improvement in gross power density realized through blending as a function of river water salinity S_r for three RED systems proposed in the literature

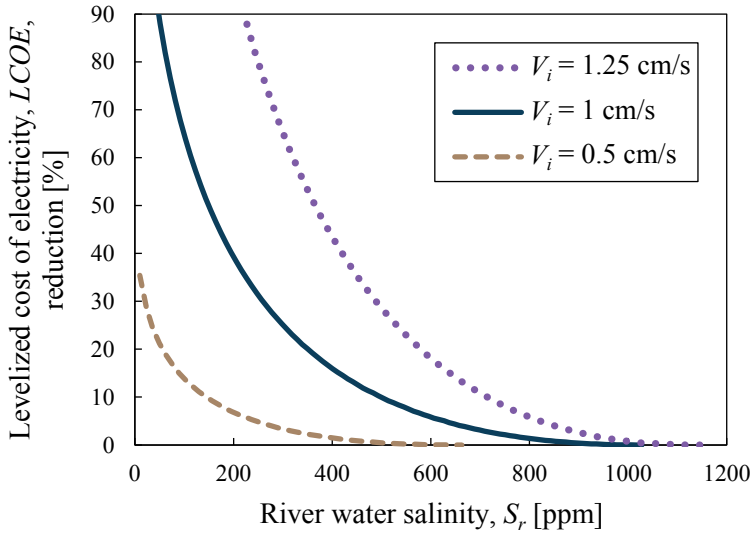

Figure 3-8: The percent reduction in the levelized cost of electricity resulting from front-end blending, as a function of river water salinity S_r for three RED systems proposed in the literature

configuration approach 100%. At river water salinities approaching the optimal inlet diluate salinity, neither form of blending offers significant cost reductions. In general, back-end blending offers higher additional cost reductions with increasing feed velocity, because the difference between the outlet and inlet diluate salinities decreases with increasing velocity

and a larger recirculation mass fraction, X_{blend} is required. See Sect. 3.4.4 for plots of the required blending mass fraction X_{blend} in both the front-end and back-end blending cases.

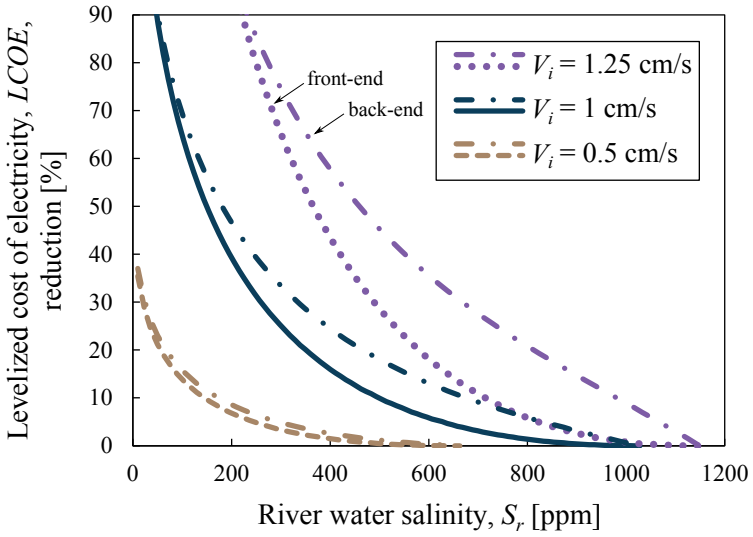

Figure 3-9: Comparison of the total percent reduction in $LCOE$ for back-end blending versus front-end blending across a range of river water salinities

3.4.4 Plots of the required blending mass fraction X_{blend}

We model front-end blending in the following way, considering a salt and mass balance:

$$C_r\phi_r + X_{\text{blend}}C_{c,i}\phi_{sw} = C_{d,i}\phi_{d,i} \tag{3.20}$$

$$\rho_r\phi_r + X_{\text{blend}}\rho_{c,i}\phi_{sw} = \rho_{d,i}\phi_{d,i} \tag{3.21}$$

where C_r is the river water concentration, ϕ_r is the river water flow rate, $C_{c,i}$ is the concentrate concentration at the stack inlet, ϕ_{sw} is the seawater flow rate, $C_{d,i}$ is the diluate concentration at the stack inlet, $\phi_{d,i}$ is the diluate flow rate at the stack inlet, $\rho_{c,i}$ is the concentrate density at the stack inlet, and $\rho_{d,i}$ is the diluate density at the stack inlet.

Figure 3-10 shows the required mass fraction X_{blend} of seawater to be blended with river water in blending to the optimal inlet diluate salinity. In the Rhone River case with a feed velocity of 1 cm/s, X_{blend} is 0.02.

The blending fractions decrease nearly linearly with river water salinity as the river salinity approaches the optimal diluate salinity. Blending fractions increase with velocity as the optimal inlet diluate salinity also increases with velocity.

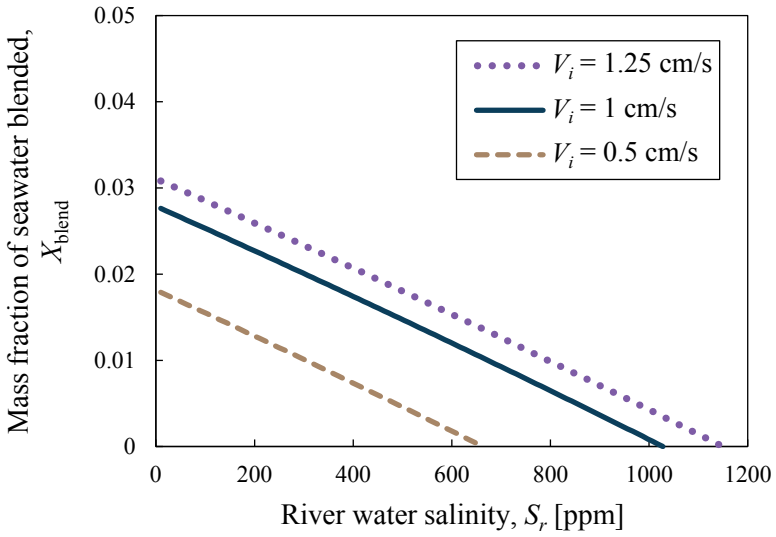

Figure 3-10: The required mass fraction of pretreated seawater to be blended with river water in the front-end blending configuration shown in Fig. 3-2

We model back-end blending with diluate recirculation in the following way, considering a salt and mass balance:

$$C_r\phi_r + X_{\text{blend}}C_{d,N}\phi_{d,N} = C_{d,i}\phi_{d,i} \tag{3.22}$$

$$\rho_r\phi_r + X_{\text{blend}}\rho_{d,N}\phi_{d,N} = \rho_{d,i}\phi_{d,i} \tag{3.23}$$

where $C_{d,N}$ is the diluate concentration at the stack exit, $\phi_{d,N}$ is the diluate flow rate at the stack exit, and $\rho_{d,N}$ is the diluate density at the stack exit.

Figure 3-11 shows the required mass fraction X_{blend} of the exiting diluate feed to be blended with river water in blending to the optimal inlet diluate salinity. In the Rhone River case with a feed velocity of 1 cm/s, X_{blend} is 0.26.

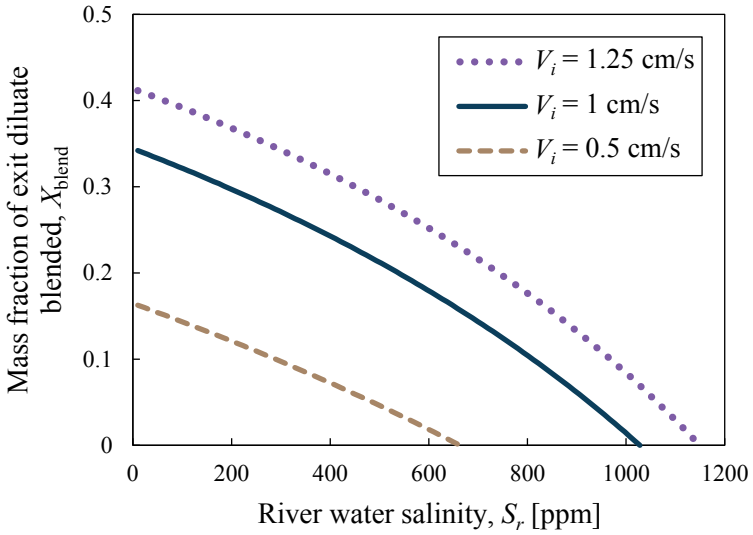

Figure 3-11: The required mass fraction of the exiting diluate stream to be blended with river water in the back-end blending configuration shown in Fig. 3-3

3.5 Discussion

3.5.1 Effect of blending on average resistances and average resistive losses

To illustrate the impact blending has on surface resistance contributions within the stack, we consider the example case of an RED stack installed on the Rhone River (339 ppm). As shown in Fig. 3-12 below, blending reduces the total average stack resistance $\bar{r}_{tot}$ by about 46%. This arises from reductions in the average diluate channel resistance $\bar{r}_{d,avg}$ (by 53%) and the average effective concentration polarization resistance $\bar{r}_{\mathrm{CP},avg}$ (by about 53%). The average concentrate channel resistance $\bar{r}_{c,avg}$ remains relatively constant (membrane resistances, $\bar{r}_{\mathrm{AEM}}$ and $\bar{r}_{\mathrm{CEM}}$, are held constant at 1 Ω cm^2).

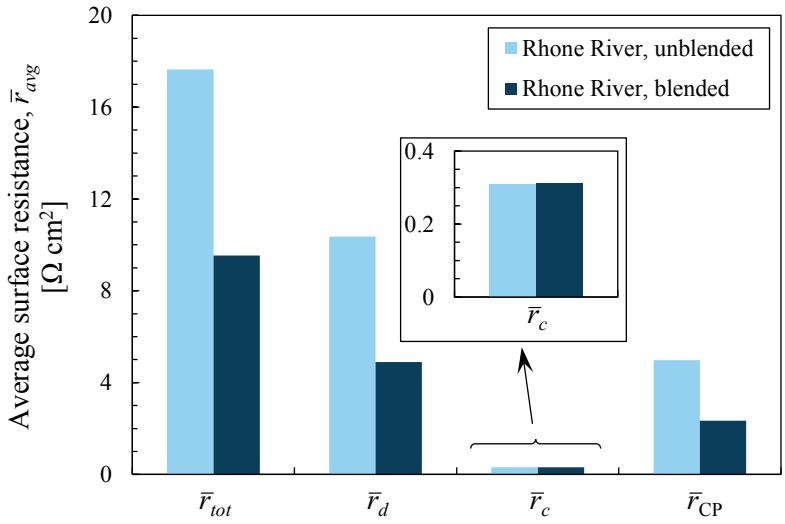

Figure 3-12: Blending significantly reduces the total stack surface resistance $\bar{r}_{tot}$ by reducing the average diluate channel resistance $\bar{r}_{d,avg}$ and the average effective concentration polarization resistance $\bar{r}_{\mathrm{CP},avg}$. Surface resistance profiles are averaged over the stack length.

3.5.2 Blending improvements at promising estuaries around the world

In Table 3.2, we evaluate the power density improvements gained through blending for RED stacks installed at promising river mouth systems throughout the world. Locations with low salt intrusion lengths [14] and mild climates where reduced sedimentation and biological activity drive pretreatment costs [5] down are most promising. Additionally, rivers with estuaries in close proximity to large population centers and in regions with favorable renewable energy policies show the most promise.

Data on river water salinities is taken from Gaillardet et al. [2] who references the GEMS/WATER Global Register of River Inputs. The Register compiles dissolved ion measurements from various sources. Each measurement is collected near the river mouth and upstream of any ocean influence and is averaged over at least five years [42]. As we are using TDS for salinity, we do not account for the effect of multivalent ions on RED power density [43]. Additionally, we assume an available seawater salinity of 35,000 ppm, although ocean salinities along coastlines may range between 30,000 and 40,000 ppm [44].

River	TDS [2]	$P_{D,g} \uparrow$	LCOE $\downarrow$
Congo	35 ppm	65%	96%
Ebro	517 ppm	4%	17%
Magdelena	118 ppm	29%	64%
Mississippi	216 ppm	17%	44%
Niger	59 ppm	48%	85%
Po	354 ppm	8%	29%
Rhone	339 ppm	9%	30%

Table 3.2: Percent power density improvements and levelized cost of electricity reductions through back-end blending at promising locations around the world, assuming an available seawater salinity of 35,000 ppm and a feed velocity of 1 cm/s

3.5.3 Impact on future designs

The power density improvements that can be gained through blending are sensitive to design parameters such as feed velocity, stack length, and channel height. Considering that RED stack designs may change with time, we evaluate how power density improvements change with respect to these design parameters.

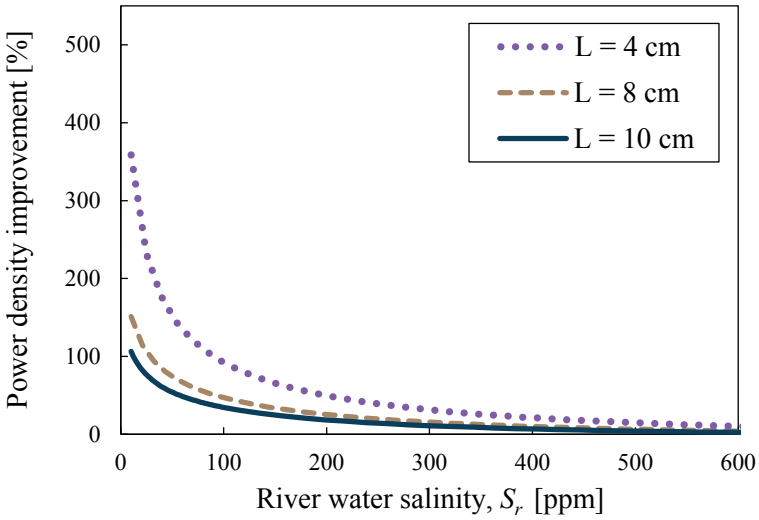

Figure 3-13: Blending improvements are sensitive to the stack length, with improvements increasing with decreasing stack length.

Figure 3-13 shows that improvements made through blending increase across all available river water salinities for designs with shorter stack lengths. For the Rhone River case (339

ppm available river water feed), decreasing the stack length from 10 cm to 4 cm increases blending improvements by about 18 percentage points. The 10 cm stack length is the prevailing length chosen in the literature [1, 18, 22] and is cost advantageous under specific conditions (i.e., available salinities, membrane prices, and pretreatment cost figures). However, as these conditions change, so may the optimal stack length. Increasing improvements through blending with decreasing stack lengths will incentivize blending in smaller stack designs.

Figure 3-14 shows increasing improvements from blending with increasing channel height. For the Rhone River case (339 ppm river water), increasing the channel height from 100 μm to 200 μm increases blending improvements by about 10 percentage points. Improvements are most sensitive to channel height, because the diluate resistance scales with channel height directly (see Eq. 3.10). The 100 μm channel height represents the optimal channel height with respect to the net power density identified in the literature (excluding pretreatment energy and capital costs) [1].

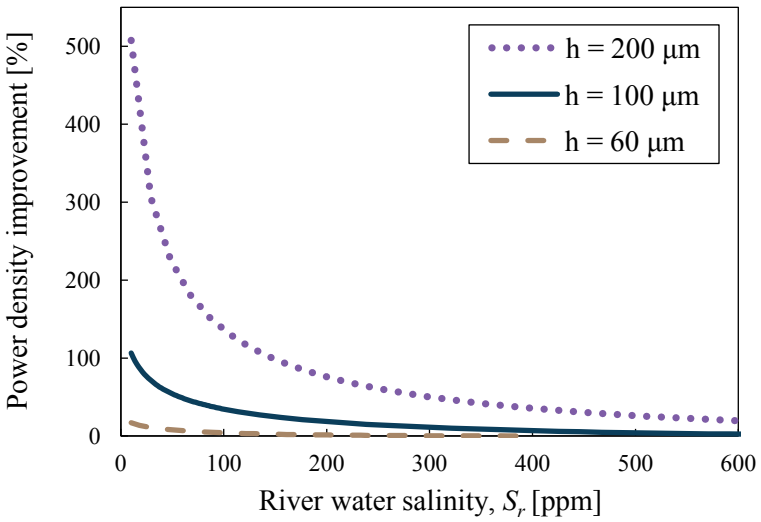

Figure 3-14: Effect of channel height on gross power density improvement for various river water salinities. Channel height has the largest impact on blending improvements, with benefits significantly decreasing with decreasing channel height.

3.6 Conclusions

Our analysis of the optimal inlet diluate salinity for current RED stack designs shows that for nearly all river mouth systems deemed suitable for salinity gradient power, blending significantly improves the gross power density and reduces the levelized cost of electricity. In the case of the RED stack sourcing river water from the Rhone (339 ppm and 1 cm/s feed velocity), a 9% increase in gross power density and 21% reduction in the levelized cost of electricity are achievable through front-end blending.

Further cost reductions may be realized by implementing back-end blending with diluate recirculation. In the case of the Rhone, a 30% total reduction in the levelized cost of electricity may be realized. Considering that stack designs may evolve with time, we predict that configurations with higher feed velocities, smaller stack lengths, and larger channel heights will benefit more from blending.

THIS PAGE INTENTIONALLY LEFT BLANK

Chapter 4

Looking Ahead

The system-level design strategy outlined in Chapter 2 provides a simple framework for determining the optimal load resistance, feed velocity, and length of an RED stack, identifying the important trade-offs for each parameter. However, the numerical results will generally vary depending mainly on local RED pretreatment energy requirements. Developing a better understanding of how these requirements vary at promising river mouths worldwide would form a worthy subject of future research.

The back-end blending design enhancement proposed in Chapter 3 shows promise based on a theoretical analysis of power density and levelized cost of electricity improvements for a typical stack. Nevertheless, the impact of blending on the optimal feed velocity and stack length remains unknown. Future research should be devoted to developing a broader design strategy which includes the blending fraction as an additional design parameter.

In this chapter, we explore the impact of the conclusions drawn in Chapters 2 and 3 on future RED stack designs, make additional recommendations on future research, and ultimately assess the viability of reverse electrodialysis now and in the future.

4.1 RED design strategy: impact and next steps

One of the key contributions of the research outlined in Chapter 2 is the development and analysis of a simple levelized cost of electricity model for RED which may be used to make stack design decisions. Previous cost models of RED were complex and focused solely on evaluating financial feasibility [16, 29]. The main impact of our cost model on stack design is the ability to use a single objective function to determine design parameters and the ability to prescribe a stack length which accounts for stack efficiency. In general, accounting for stack efficiency will drive optimal residence times (and stack lengths) in future designs higher.

Another utility of the cost model developed and the optimization procedure proposed is the ability to examine how stack designs will change in the future as membrane prices decrease over time. An advantage of our methodology is that optimal load resistances and feed velocities will remain the same regardless of membrane prices and only stack residence times will change. An examination of this change is presented in Fig. 4-1 where each curve represents how the levelized cost of electricity varies with residence time for a particular capital cost figure K_{mem}.

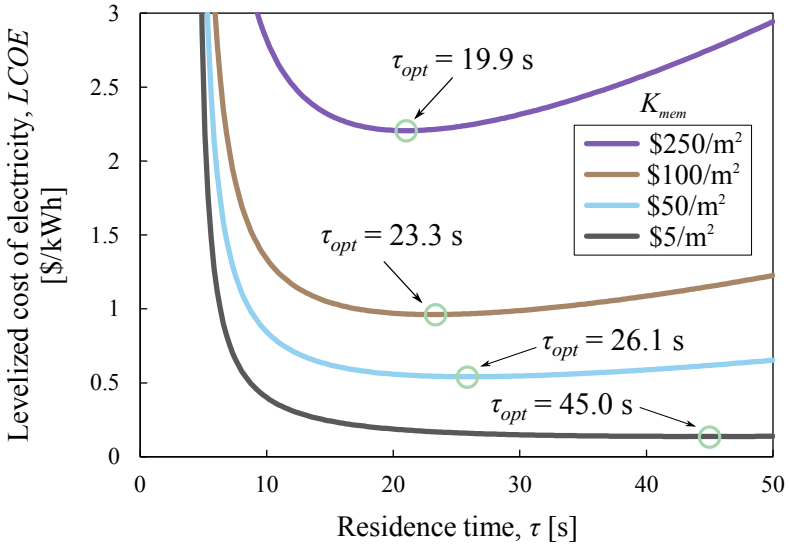

Figure 4-1: The change in the optimal residence time as the capital cost figure K_{mem} decreases over time

As membrane prices decrease, the relative capital cost contribution of the pretreatment

system increases. Because cost-effective pretreatment systems favor long stack lengths, the optimal residence time increases. For a capital cost figure of \$5/m^2, which is the target according to Daniilidis et al. [16] for RED to compete with other renewables, the optimal residence time is 45.0 s. With an optimal feed velocity of 0.46 cm/s this corresponds to a stack length of 21 cm. The levelized cost of electricity is \$0.14/kWh.

Future stacks will also feature load resistances which are optimized as opposed to matched to the equivalent stack resistance. This will drive load resistances down. Additionally, as membrane prices fall and the optimal residence time increases, the importance of optimizing the load as opposed to matching it will increase. Figure 4-2 shows the discrepancy in gross power density between load optimization and load matching over a range of optimal residence times. The discrepancy increases as the optimal residence time increases.

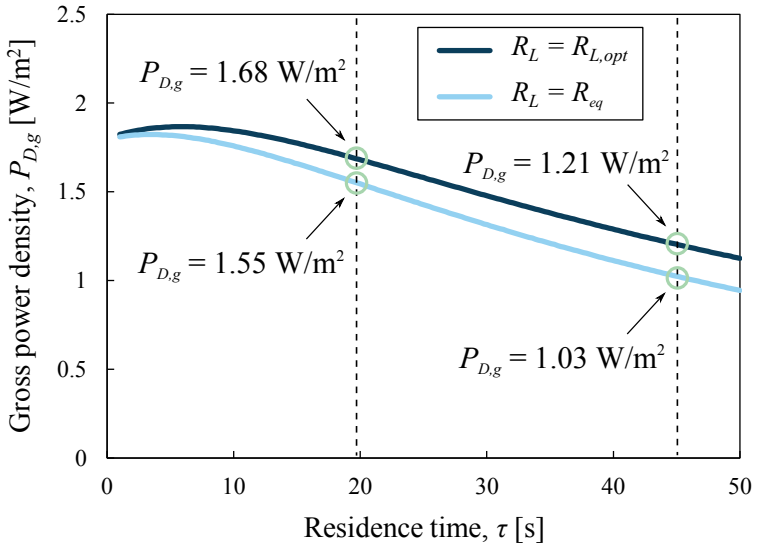

Figure 4-2: The change in gross power density with optimal residence time for load resistance optimization and load resistance matching

While the importance of optimizing the load resistance increases with decreasing membrane price, Chapter 2 shows that regardless of membrane price, maintaining low pretreatment and pumping energy requirements is vital. A strong understanding of these requirements is also critical to making sound design decisions. While a recent study by Pawlowski et al. [45] explores pumping energy requirements through RED stacks, a detailed study on

pretreatment requirements for RED systems and how these requirements vary at promising river mouth sites around the world would be valuable as the subject of future research. The results could easily be integrated into the design strategy outlined in Chapter 2, producing accurate design recommendations at specific locations.

4.2 RED blending design: impact and next steps

Beyond offering and analyzing a design enhancement which can significantly increase the power density and lower the levelized cost of electricity, Chapter 3 highlights the importance of understanding and monitoring the salinity of the river water feed for any stack design. As the feed salinities may vary widely across wet and dry seasons through the year [46], future RED systems should employ salinity monitoring and dynamic blending capabilities to minimize the levelized cost of electricity. As we show in Chapter 3, the consideration is especially important for low salinity rivers. Other design enhancements which could be developed and explored in future research include the management of storage capabilities and/or adaptable withdrawal systems to account for temporal and spatial salinity variations. Additionally, studies evaluating the impact of RED withdrawal and discharge on salinity structures in river mouths should also be investigated in more detail.

The research presented in Chapter 3 also raises questions on whether thorough pretreatment is preferable to periodic membrane cleaning techniques such as air-sparging and feedwater reversal or to what degree these processes should be integrated. With back-end blending there is added value to pretreating the river water, as the recycling of pretreated diluate for blending results in sizable cost reductions. While studies have shown the effectiveness of air-sparging and feedwater reversal in RED for cleaning the membranes [13], they have not analyzed the energy and capital costs of these methodologies nor have they compared them to pretreatment costs and benefits, especially after considering back-end blending.

The consideration of back-end blending should also form part of a broader RED design optimization and an investigation into the impact on the optimal load resistance, feed veloc-

ity, and residence time is necessary. As was shown in Chapter 3, the trade-offs determining the optimal back-end blending fraction X_{blend} are complex. There exists not only the standard trade-off between stack voltage and stack resistance with respect to maximizing the gross power density, but also the pretreatment capital cost reduction and the pretreatment energy reduction associated with increased blending. Consequently, a more comprehensive design optimization is required.

4.3 Assessment of RED viability

Despite the design enhancements and strategies presented in this research, at current system capital costs reverse electrodialysis is not an economically viable renewable energy technology in most scenarios. The dominating factor currently is the high membrane price [16]. Despite the seemingly precipitous fall in membrane price required to make RED viable, there are several reasons why I remain optimistic that RED will continue to garner significant attention and compete with other renewable technologies in the future.

4.3.1 Renewable technologies are gaining ground

Global renewable energy capacity increased by more than 8% in 2013, largely driven by increased efficiency, but also a result of heavy investments made by governments like China, who poured more than $56 billion into the clean energy industry [47]. In many countries, renewable technologies have become a significant part of the energy portfolio. From my perspective, a healthy renewable energy market which is attracting significant money is a boon to the development of more fringe renewable energy technologies such as RED. To some extent, the increased investment indicates a general prioritization of environmental concerns associated with electricity production worldwide. At the same time, each renewable energy technology has distinct shortcomings and a suitability to specific applications which makes the exploration of a wide variety of technologies (among them, RED) worthwhile.

4.3.2 Distinct advantages

As was highlighted in Chapter 1, reverse electrodialysis has distinct advantages relative to other renewable technologies. Among these are the non-intermittent production, the absence of waste streams and emissions in operation, and potentially lower environmental and social impacts than hydroelectric power. Specifically, RED plants could be less disruptive to the landscape than wind farms and completely avoid storage issues associated with solar fields.

4.3.3 Falling membrane prices

While membranes tailored to RED, with a lower resistance and higher permselectivity than ED membranes, cost more than $\$100/m^2$ [33] today, there is reason to believe that membrane prices will continue to decline. Commercial heterogeneous ion exchange membranes are currently available for less than $\$4.50/m^2$ [33], and with desalination plants becoming more widespread the capital cost of RED plants, which share similar characteristics with traditional seawater desalination plants, will continue to fall.

4.3.4 Potential impact of innovations

Promising advancements in reverse electrodialysis will also drive down the levelized cost of electricity. One such advancement is the development of profiled membranes [20] which eliminates the need for spacers, nearly halves the channel resistance, and significantly reduces the required pumping power. Innovative manufacturing techniques for producing such membranes are also being developed [48]. Other advancements in RED include the development of monovalent ion selective membranes to reduce power density losses attributed to multivalent ion transport [49]. Multivalent ions in various feedwaters, including river and sea water, reduce the stack power density by increasing the membrane resistance and by transporting against their concentration gradient, lowering the stack voltage. This arises, because the membranes have a low selectivity towards multivalent ions. Altogether the design and development of the RED stack is a vibrant research space which will continue to attract more

attention as costs come down.

Beyond innovations within the RED stack, researchers are beginning to systematically analyze the potential of RED implementation at specific river mouths around the world [14, 46]. This research, along with research centering around new applications beyond traditional sea and river water power generation, is helping to hone in on the most favorable opportunities for RED.

4.3.5 Other applications

A major new application for RED is energy recovery from industrial waste streams. A closed-loop ammonium bicarbonate-based reverse electrodialysis system has been developed to generate electricity while neutralizing waste acid and producing hydrogen [50]. In a similar closed-loop system, microbial reverse electrodialysis cells (MRCs) have also been developed to recover energy from wastewater [51].

Smaller scale applications include the powering of micro and nano devices without batteries or external power supplies. An RED-powered microfluidic platform built from self-assembled nanoparticles has been demonstrated [52]. The device offers a power density and efficiency which is tunable based on the geometry of the nanochannels.

A deeper analysis of the efficiency of such processes and cost comparisons with existing solutions should form the basis of future research. Additionally, insights from the research presented in this thesis could help guide better stack designs for each of these future applications.

THIS PAGE INTENTIONALLY LEFT BLANK

References

[1] D. A. Vermaas, M. Saakes, and K. Nijmeijer. Doubled power density from salinity gradients at reduced intermembrane distance. *Environmental Science and Technology*, 45(16):7089–7095, 2011.

[2] J. Gaillardet, B. Dupré, P. Louvat, and C. J. Allegre. Global silicate weathering and CO_2 consumption rates deduced from the chemistry of large rivers. *Chemical Geology*, 159(1):3–30, 1999.

[3] A. G. Konings, X. Feng, A. Molini, S. Manzoni, G. Vico, and A. Porporato. Thermodynamics of an idealized hydrologic cycle. *Water Resources Research*, 48(5), 2012.

[4] J. Veerman, M. Saakes, S. J. Metz, and G. J. Harmsen. Reverse electrodialysis: evaluation of suitable electrode systems. *Journal of Applied Electrochemistry*, 40(8):1461–1474, 2010.

[5] D. A. Vermaas. *Energy generation from mixing salt water and fresh water: Smart flow strategies for reverse electrodialysis*. PhD thesis, University of Twente, 2013. http://www.waddenacademie.nl.

[6] G. L. Wick and W. R. Schmitt. Prospects for renewable energy from sea. *Marine Technology Society Journal*, 11(5-6):16–21, 1977.

[7] J. W. Post, H. V. M. Hamelers, and C. J. N. Buisman. Energy recovery from controlled mixing salt and fresh water with a reverse electrodialysis system. *Environmental Science and Technology*, 42(15):5785–5790, 2008.

[8] Bureau of Reclamation. Hydroelectric power. Technical report, United States Department of the Interior, 2005.

[9] US Army Corps of Engineers. National inventory of dams, February 2013. geo.usace.army.mil.

[10] Hydropower in Vietnam: Full to bursting. *The Economist*, 2015.

[11] K. Kontturi, L. Murtomäki, and J. A. Manzanares. *Ionic Transport Processes: in Electrochemistry and Membrane Science: in Electrochemistry and Membrane Science*. Oxford University Press, 2008.

[12] J. W. Post, J. Veerman, H. V. M. Hamelers, G. J. W. Euverink, S. J. Metz, K. Nymeijer, and C. J. N. Buisman. Salinity-gradient power: Evaluation of pressure-retarded osmosis and reverse electrodialysis. *Journal of Membrane Science*, 288(1):218–230, 2007.

[13] D. A. Vermaas, D. Kunteng, J. Veerman, M. Saakes, and K. Nijmeijer. Periodic feedwater reversal and air sparging as antifouling strategies in reverse electrodialysis. *Environmental Science & Technology*, 48(5):3065–3073, 2014.

[14] O. Alvarez-Silva, C. Winter, and A. F. Osorio. Salinity gradient energy at river mouths. *Environmental Science & Technology Letters*, 1(10):410–415, 2014.

[15] M. Janssen, A. Härtel, and R. van Roij. Boosting capacitive blue-energy and desalination devices with waste heat. *Physical Review Letters*, 2015.

[16] A. Daniilidis, D. A. Vermaas, R. Herber, and K. Nijmeijer. Experimentally obtainable energy from mixing river water, seawater or brines with reverse electrodialysis. *Renewable Energy*, 64:123–131, 2014.

[17] N. Y. Yip, D. A. Vermaas, K. Nijmeijer, and M. Elimelech. Thermodynamic, energy efficiency, and power density analysis of reverse electrodialysis power generation with natural salinity gradients. *Environmental Science and Technology*, 48(9):4925–4936, 2014.

[18] J. Veerman, M. Saakes, S. J. Metz, and G. J. Harmsen. Reverse electrodialysis: A validated process model for design and optimization. *Chemical Engineering Journal*, 166(1):256–268, 2011.

[19] E. Güler, R. Elizen, D. A. Vermaas, M. Saakes, and K. Nijmeijer. Performance-determining membrane properties in reverse electrodialysis. *Journal of Membrane Science*, 446:266–276, 2013.

[20] D. A. Vermaas, M. Saakes, and K. Nijmeijer. Power generation using profiled membranes in reverse electrodialysis. *Journal of Membrane Science*, 385:234–242, 2011.

[21] P. Dlugolecki, B. Anet, S. J. Metz, K. Nijmeijer, and M. Wessling. Transport limitations in ion exchange membranes at low salt concentrations. *Journal of Membrane Science*, 346(1):163–171, 2010.

[22] D. A. Vermaas, E. Guler, M. Saakes, and K. Nijmeijer. Theoretical power density from salinity gradients using reverse electrodialysis. *Energy Procedia*, 20:170–184, 2012.

[23] S. Klein and F. Alvarado. Engineering equation solver, F-Chart software, 2014.

[24] R. K. McGovern, S. M. Zubair, and J. H. Lienhard V. The cost effectiveness of electrodialysis for diverse salinity applications. *Desalination*, 348:57–65, 2014.

[25] O. Kuroda, S. Takahashi, and M. Nomura. Characteristics of flow and mass transfer rate in an electrodialyzer compartment including spacer. *Desalination*, 46(1):225–232, 1983.

[26] J. F. Chambers, J. M. Stokes, and R. H. Stokes. Conductances of concentrated aqueous sodium and potassium chloride solutions at 25C. *The Journal of Physical Chemistry*, 60(7):985–986, 1956.

[27] M. Fidaleo and M. Moresi. Optimal strategy to model the electrodialytic recovery of a strong electrolyte. *Journal of Membrane Science*, 260(1):90–111, 2005.

[28] R. R. A. Robinson and R. R. H. Stokes. *Electrolyte solutions*. Courier Dover Publications, 2002.

[29] J. W. Post, C. H. Goeting, J. Valk, S. Goinga, J. Veerman, H. V. M. Hamelers, and P. J. F. M. Hack. Towards implementation of reverse electrodialysis for power generation from salinity gradients. *Desalination and Water Treatment*, 16(1-3):182–193, 2010.

[30] R. K. McGovern, A. M. Weiner, L. Sun, C. G. Chambers, S. M. Zubair, and J. H. Lienhard V. On the cost of electrodialysis for the desalination of high salinity feeds. *Applied Energy*, 136:649–661, 2014.

[31] Environmental Protection Agency. Technology and cost document for the final ground water rule, October 2006. http://www.epa.gov/.

[32] R. K. McGovern, S. M. Zubair, and J. H. Lienhard V. The benefits of hybridising electrodialysis with reverse osmosis. *Journal of Membrane Science*, 469:326–335, 2014.

[33] M. Turek and B. Bandura. Renewable energy by reverse electrodialysis. *Desalination*, 205(1):67–74, 2007.

[34] M. Fidaleo and M. Moresi. Electrodialytic desalting of model concentrated NaCl brines as such or enriched with a non-electrolyte osmotic component. *Journal of Membrane Science*, 367(1):220–232, 2011.

[35] P. Dlugolecki, A. Gambier, K. Nijmeijer, and M. Wessling. Practical potential of reverse electrodialysis as process for sustainable energy generation. *Environmental Science & Technology*, 43(17):6888–6894, 2009.

[36] J. N. Weinstein and F. B. Leitz. Electric power from differences in salinity: the dialytic battery. *Science*, 191(4227):557–559, 1976.

[37] R. E. Lacey. Energy by reverse electrodialysis. *Ocean Engineering*, 7(1):1–47, 1980.

[38] R. K. McGovern, S. M. Zubair, and J. H. Lienhard V. Hybrid electrodialysis reverse osmosis system design and its optimization for treatment of highly saline brines. *IDA Journal of Desalination and Water Reuse*, 6(1):15–23, 2014.

[39] S. Loeb. Energy production at the Dead Sea by pressure-retarded osmosis: challenge or chimera? *Desalination*, 120(3):247–262, 1998.

[40] J. Veerman, J. W. Post, M. Saakes, S. J. Metz, and G. J. Harmsen. Reducing power losses caused by ionic shortcut currents in reverse electrodialysis stacks by a validated model. *Journal of Membrane Science*, 310(1):418–430, 2008.

[41] K. S. Pitzer, J. C. Peiper, and R. H. Busey. *Thermodynamic properties of aqueous sodium chloride solutions.* American Chemical Society and the American Institute of Physics for the National Bureau of Standards, 1984.

[42] M. Meybeck and A. Ragu. *River discharges to the oceans: an assessment of suspended solids, major ions and nutrients.* UNEP, 1997.

[43] J. W. Post, H. V. M. Hamelers, and C. J. N. Buisman. Influence of multivalent ions on power production from mixing salt and fresh water with a reverse electrodialysis system. *Journal of Membrane Science*, 330(1):65–72, 2009.

[44] L. Jenner. Aquarius: Studying our salty seas from space, September 2013. http://www.nasa.gov/mission_pages/aquarius.

[45] S. Pawlowski, J. G. Crespo, and S. Velizarov. Pressure drop in reverse electrodialysis: Experimental and modeling studies for stacks with variable number of cell pairs. *Journal of Membrane Science*, 462:96–111, 2014.

[46] O. Alvarez-Silva and A. F. Osorio. Salinity gradient energy potential in Colombia considering site specific constraints. *Renewable Energy*, 74:737–748, 2015.

[47] Renewables: We make our own. *The Economist*, 2015.

[48] E. Güler, R. Elizen, M. Saakes, and K. Nijmeijer. Micro-structured membranes for electricity generation by reverse electrodialysis. *Journal of Membrane Science*, 458:136–148, 2014.

[49] E. Güler, W. van Baak, M. Saakes, and K. Nijmeijer. Monovalent-ion-selective membranes for reverse electrodialysis. *Journal of Membrane Science*, 455:254–270, 2014.

[50] M. C. Hatzell, X. Zhu, and B. E. Logan. Simultaneous hydrogen generation and waste acid neutralization in a reverse electrodialysis system. *ACS Sustainable Chemistry & Engineering*, 2(9):2211–2216, 2014.

[51] R. D. Cusick, Y. Kim, and B. E. Logan. Energy capture from thermolytic solutions in microbial reverse-electrodialysis cells. *Science*, 335(6075):1474–1477, 2012.

[52] E. Choi, K. Kwon, D. Kim, and J. Park. Tunable reverse electrodialysis microplatform with geometrically controlled self-assembled nanoparticle network. *Lab on a Chip*, 15(1):168–178, 2015.